



Self-thermoelectrophoresis at low salinity†

Joost de Graaf * and Sela Samin

Cite this: *Soft Matter*, 2019, 15, 7219

Received 1st May 2019,
Accepted 15th August 2019

DOI: 10.1039/c9sm00886a

rsc.li/soft-matter-journal

A locally heated Janus colloid can achieve motion in an electrolyte by an effect known as self-thermo(di)electrophoresis. We numerically study the self-propulsion of such a “hot swimmer” in a monovalent electrolyte using the finite-element method and analytic theory. The effect of electrostatic screening for intermediate and large Debye lengths is charted and we report on the fluid flow generated by self-thermoelectrophoresis. We obtain excellent agreement between our analytic theory and numerical calculations in the limit of high salinity, validating our approach. At low salt concentrations, we employ Teubner’s integral formalism to arrive at expressions for the speed, which agree semi-quantitatively with our numerical results for conducting swimmers. This lends credibility to the remarkably high swim speed at very low ionic strength, which we numerically obtain for a fully insulating swimmer. We also report on hot swimmers with a mixed electrostatic boundary conditions. Our results should benefit the realization and analysis of further experiments on thermo(di)electrophoretic swimmers.

1 Introduction

Nearly a decade and a half ago saw the introduction of the first man-made chemical swimmers, colloidal particles that used catalytic decomposition of hydrogen peroxide (H_2O_2) to achieve self-propulsion.^{1,2} These Janus swimmers were heralded as artificial model systems for studying the complex motion and cooperative behavior observed in biology,³ such dynamics have by now indeed been reproduced in man-made systems.^{4–8} Nevertheless, despite the success of these chemical swimmers, many open problems remain regarding their application.

For example, H_2O_2 is detrimental to biological systems, as are many other catalytic fuels,^{9,10} which limits their potential for *in vivo* use. This has led to the exploration of other self-propulsion strategies, which involve biocompatible surface chemistry.^{11,12} A promising alternative to chemical self-propulsion is thermophoresis,^{13–16} which utilizes local heating to achieve motion through the migration of solute species in a temperature gradient. The underlying Soret effect can make use of solutes already present in the local environment and does not require large temperature gradients; it may therefore be compatible with living systems.

From a theoretical perspective, there remain open questions concerning the microscopic origins of the thermophoretic effect and associated Soret coefficients,¹⁷ seeing very recent

attempts to unify thermophoretic theory for colloidal motion.¹⁸ Significant progress has, however, been made theoretically for a specific thermal driving mechanism, where the dominant contribution comes from electrostatic interactions, *i.e.*, thermoelectrophoresis.^{16,19–25} In addition, thermophoretic theory has been used to clarify experimental results, *e.g.*, see ref. 16 and 26–29. Yet most thermo(di)electrophoretic theory considers the limit of high salt concentration, for which several well-established analytic methods may be used to derive results.

In this paper, we theoretically study self-propulsion *via* thermo(di)electrophoresis, for which we go beyond the thin-screening-layer (Smoluchowski-limit) approximations made in previous works.^{16,21,24} We describe in detail the associated equation system and solve it using the finite-element method (FEM) over the full range of experimentally relevant ion concentrations, from the Smoluchowski to the Hückel (low-salt) limit. Our calculations show motility reversals that are reminiscent of those found in external electrophoresis³⁰ and those recently reported for external thermodielectrophoresis.²⁵

We obtain self-propulsion speeds of a few $\mu\text{m s}^{-1}$ for physiologically relevant salt (monovalent ions) concentrations $\approx 1 \text{ mmol L}^{-1}$ and small local heating of $\Delta T \lesssim 5 \text{ K}$, in agreement with the literature. Changing the ions and bulk salt concentration also allows for sensitive tuning of the speed and flow field around the hot swimmer by controlling the Seebeck effect,³¹ for which we explore the impact of low conductivity of the medium, *i.e.*, low bulk salt concentration or equivalently ionic strength.

We complement our FEM results for the swim speed with analytic theory. This is based on an expansion both in terms of small temperature gradients, and in terms of small (gradients of) ion concentrations and potentials. We show that full linearization

Institute for Theoretical Physics, Center for Extreme Matter and Emergent Phenomena, Utrecht University, Princetonplein 5, 3584 CC Utrecht, The Netherlands. E-mail: j.degraaf@uu.nl

† Electronic supplementary information (ESI) available: Mathematical notebooks that provide the analytic derivation for the intermediate regime of reservoir salt concentration, as well as an evaluated pdf version. See DOI: 10.1039/c9sm00886a

in both expansions is not possible and that cross terms between equilibrium and out-of-equilibrium expansion fields must be preserved in order to account for thermo(di)electrophoretic self-propulsion. Within our partial linearization approximation, we determine the swim speed using both the slip-layer approximation and an integral formalism based on reciprocity, originally developed by Teubner.³² The latter allows for direct evaluation of the swim speed from the body-force distribution, without imposing constraints on the size of the screening layer with respect to the colloid. We obtain agreement between both approaches in the Smoluchowski limit, which also match our FEM results well. Our analytic expressions for the speed fortuitously hold even when the concentration profiles and charge excess are no longer well captured by the same approximative theory.

The generality of Teubner's formalism allows us to tackle the regime of intermediate to low ionic strength. We use two analytic approaches for studying the departures from the Hückel limit. The first is based on regime splitting. The potential is assumed to be unscreened up to roughly the Debye length, which must be very large in order to make this approximation; the potential is set to zero outside of this range. The second approach uses an ansatz for the temperature distribution around the swimmer. That is, we only take into account the dipolar contribution of the full Legendre–Fourier series, in which we can expand the temperature field. This contribution is the one that generates the speed, and ignoring the other components greatly reduces complexity of the involved mathematics, though the calculations remain laborious.

Our two approaches give similar results near the Hückel limit and we discuss the origin of the differences. For an equipotential swimmer, our analytic results hold incredibly well even in the intermediate regime of ionic strength, when compared to our more accurate FEM calculations. For an insulating swimmer, only the Smoluchowski limit is well captured. This is to be expected, due to the difference in boundary conditions, which makes the low-ionic strength situation difficult to tackle analytically. Nonetheless, we are confident in our numerically obtained value of a measurably high self-propulsion speed for an insulating hot swimmer at low ionic strength. We further use our numerical method to explore the robustness of this finding to mixed electrostatic boundary conditions, which could be more representative of experiment. Our proof-of-principle calculations do not show a “best of both worlds” scenario, wherein the speed is high over the entire range of ionic strength, though it cannot be excluded in its entirety on the basis of our present analysis.

The analytic and numerical work performed in this paper provide a solid background against which more detailed investigations of self-thermo(di)electrophoretic effects can be realized. This may also guide future experiments in selecting optimal conditions for self-propulsion using this mechanism and in manipulating the swimmers' motility using ionic strength alone.

The remainder of this manuscript is structured as follows. In Section 2 we introduce the model system. Section 3 provides the linearization of the equation system that governs the

self-thermo(di)electrophoretic motion. Section 4 obtains swim speeds from these linearized expressions in the Smoluchowski limit. Section 5 details our analytic calculations based on Teubner's formalism around the Hückel limit. Lastly, Section 6 provides an analysis of the speed for intermediate ionic strengths. The analytic sections are lengthy and algebra heavy and readers primarily interested in the numerical results are therefore recommended to skip ahead to Section 7. We summarize, discuss, and provide an outlook in Section 8.

2 The model

We consider a single spherical colloid of radius a half-coated by a thin metal or carbon cap. The colloid is immersed in an electrolyte, comprised of water and a monovalent salt, with reservoir concentration n^∞ and local salinities $n_\pm(\vec{r})$, where \vec{r} is the position vector. By illuminating the colloid with an appropriately chosen light source, the cap can be heated, which leads to a temperature heterogeneity around the colloid which drives the system out of equilibrium. This causes the colloid to self-propel due to the thermoelectrophoresis, see Fig. 1 for a schematic illustration. Here, we also define our radial r and axial z coordinates (unit vectors \hat{r} and \hat{z} , respectively), as well as the polar angle θ .

The governing equations of our system in steady state are as follows. The temperature distribution throughout the system is given by $T(\vec{r})$ and obeys the heat equation,

$$\vec{\nabla} \cdot [k(T(\vec{r}))\vec{\nabla}T(\vec{r})] = 0, \quad (1)$$

where k is the thermal conductivity, with $k = k_f$ in the fluid and $k = k_s$ for the solid colloid. In eqn (1), we neglected advection in the fluid phase since the typical $\mathcal{O}(\mu\text{m s}^{-1})$ velocities of microswimmers lead to small thermal Péclet numbers, *i.e.*, thermal diffusion dominates thermal advection. Note that we take the thermal conductivity in eqn (1) to be temperature dependent, with the constitutive relation for $k(T)$ given in Section 3. Temperature dependence will be considered for all physical properties in this work, however, we leave the $T(\vec{r})$ dependence of all fields, *e.g.*, the fluid velocity and potential, implicit throughout. This way of writing the functional dependence

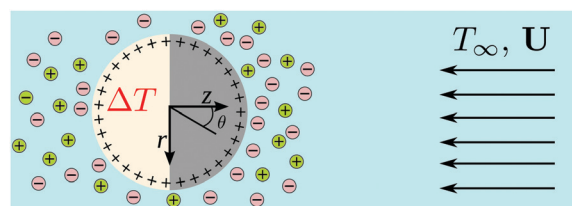


Fig. 1 Sketch of a charged Janus particle (axisymmetric around z) immersed in an electrolyte with an ambient temperature T_∞ . Illumination of the capped hemisphere (light yellow; $z < 0$) increases its temperature by ΔT . In steady state, the heating leads to an asymmetric distribution of ions around the colloid, resulting in its self-propulsion. In the co-moving reference frame, the fluid velocity is then $-\vec{U}$ at infinity.

of the quantities makes the notation in this section rather heavy, but once the system is linearized it will be considerably reduced.

Within a continuum framework, the ion dynamics is captured by the classical Poisson–Nernst–Planck equations. The Poisson equation for the electric potential $\Phi(\vec{r})$ reads

$$\vec{\nabla} \cdot [\varepsilon(T(\vec{r}))\vec{\nabla}\Phi(\vec{r})] = -e[n_+(\vec{r}) - n_-(\vec{r})], \quad (2)$$

where ε is the medium's dielectric permittivity and e is the elementary charge. The Nernst–Planck equations for the ion fluxes are^{21,23}

$$\begin{aligned} \vec{j}_{\pm}(\vec{r}) = & -D_{\pm}(T(\vec{r})) \left[\vec{\nabla}n_{\pm}(\vec{r}) \pm \frac{en_{\pm}(\vec{r})}{k_{\text{B}}T(\vec{r})} \vec{\nabla}\Phi(\vec{r}) \right. \\ & \left. + 2n_{\pm}(\vec{r})\alpha_{\pm}(T(\vec{r})) \frac{\vec{\nabla}T(\vec{r})}{T(\vec{r})} \right], \end{aligned} \quad (3)$$

where k_{B} is Boltzmann's constant, D_{\pm} are the regular diffusion constants, and α_{\pm} are the thermal diffusion factors of the respective ions. The latter are related to the intrinsic Soret coefficients *via* $S_{\pm} = 2\alpha_{\pm}/T$; here we incorporate a factor 2 with respect to the usual literature convention to help compact our expressions. The equation system is closed by the ionic conservation laws

$$\vec{\nabla} \cdot \vec{j}_{\pm}(\vec{r}) = 0, \quad (4)$$

where we have employed the low-Péclet-number approximation to eliminate advective ion transport. That is, regular diffusion dominates advection, see Appendix A for the justification.

For a micron-size colloid self-propelling in water at a speed that is $\mathcal{O}(1 \mu\text{m s}^{-1})$, the relevant Reynolds number $\text{Re} \ll 1$. The fluid velocity is thus governed by the Stokes equations for an incompressible fluid

$$\begin{aligned} \eta(T(\vec{r}))\underline{\Delta}\vec{u}(\vec{r}) - \vec{\nabla}p(\vec{r}) = & e[n_+(\vec{r}) - n_-(\vec{r})]\vec{\nabla}\Phi(\vec{r}) \\ & + \frac{1}{2} \left| \vec{\nabla}\Phi(\vec{r}) \right|^2 \frac{\partial\varepsilon(T(\vec{r}))}{\partial T(\vec{r})} \vec{\nabla}T(\vec{r}); \end{aligned} \quad (5)$$

$$\vec{\nabla} \cdot \vec{u}(\vec{r}) = 0, \quad (6)$$

where η is the viscosity of the solvent and $p(\vec{r})$ is the hydrostatic pressure; $\underline{\Delta}$ indicates the vector Laplacian. Here, we use in the right-hand side of eqn (5) the body-force terms derived by Landau and Lifshits³³ and also employed by ref. 24 and 34–36, where the first term is the electric body force, which implicitly depends on the temperature through the ionic distributions, and the second term is the thermoelectric coupling due to the permittivity dependence on temperature.

The boundary conditions for our problem are as follows. We choose a frame of reference co-moving with the particle such that the fluid velocity far away from the particle obeys $\vec{u}(|\vec{r}| \uparrow \infty) = -\vec{U}$, with \vec{U} the swim velocity and $U = \vec{U} \cdot \hat{z}$ the swim speed. On the swimmer, we have a no-slip condition for the fluid velocity, $\vec{u}(\vec{r}_{\text{s}}) = \vec{0}$, where \vec{r}_{s} is a position vector on the surface of the swimmer; $|\vec{r}_{\text{s}}| = a$. N.B. Our definition of the 'swim speed' allows it to assume negative values, which we use to identify the direction of travel.

The Poisson equation has the boundary condition that the electrostatic potential decays to zero in the bulk, *i.e.*, $\Phi(|\vec{r}| \uparrow \infty) = 0$. At the surface, we must distinguish between a conductor and an insulator. For the former, we have $\Phi(\vec{r}_{\text{s}}) = \Phi_0(\vec{r}_{\text{s}})$, with Φ_0 the surface potential. For the latter, we have

$$\hat{n}(\vec{r}_{\text{s}}) \cdot \vec{\nabla}\Phi(\vec{r}) \Big|_{\vec{r}=\vec{r}_{\text{s}}} = -\sigma(\vec{r}_{\text{s}})/\varepsilon(T(\vec{r}_{\text{s}})), \quad (7)$$

where σ is the surface charge density and \hat{n} is the outward unit normal to the surface.‡

At the surface, we employ no-penetration boundary conditions for the ionic species: $\hat{n}(\vec{r}_{\text{s}}) \cdot \vec{j}_{\pm}(\vec{r}_{\text{s}}) = 0$. Fluxes parallel to the wall are permitted, *i.e.*, there is no drag. The salt concentrations at the edge of the system assume their reservoir value, $n_{\pm}(|\vec{r}| \uparrow \infty) = n^{\infty}$.

Finally, for the heat equation, the temperature far away is given by the reservoir temperature $T(|\vec{r}| \uparrow \infty) = T^{\infty}$. For the capped surface we must distinguish between constant heat flux and constant temperature, respectively. That is, we do not explicitly resolve the material of the cap in our calculations, rather we employ a constant-temperature or a constant-heat-flux surface boundary condition. To connect the physical difference in cap material to the appropriate boundary condition, we shall refer to the thermal conductivity of the cap k_{cap} in the following.

Whenever k_{cap} is much larger than that of the fluid and solid colloid, k_{f} and k_{s} , respectively, there is a constant temperature on the capped hemisphere $T(\vec{r}_{\text{s}}) = T^{\infty} + \Delta T$, with ΔT the excess temperature induced by heating. This typically occurs for a metallic cap;^{6,14} for which the value k_{cap} is typically a few hundred times larger than that of the surrounding water and colloid. When thermal conductivity of the coating is much smaller than that of the fluid and colloid, $k_{\text{cap}} \ll k_{\text{f}}, k_{\text{s}}$, *e.g.*, for a carbon coating,³⁷ heat is immediately conducted to the surroundings such that the illumination leads to a constant heat flux Q through the cap. In this case, the boundary condition for the capped region reads

$$k_{\text{s}}\hat{n}(\vec{r}_{\text{s}}) \cdot \vec{\nabla}T(\vec{r}) \Big|_{\vec{r}=\vec{r}_{\text{s}}} - k_{\text{f}}\hat{n}(\vec{r}_{\text{s}}) \cdot \vec{\nabla}T(\vec{r}) \Big|_{\vec{r}=\vec{r}_{\text{s}}} = Q(\vec{r}_{\text{s}}), \quad (8)$$

while on the uncapped half of the colloid, we have the flux continuity condition

$$k_{\text{s}}\hat{n}(\vec{r}_{\text{s}}) \cdot \vec{\nabla}T(\vec{r}) \Big|_{\vec{r}=\vec{r}_{\text{s}}} = k_{\text{f}}\hat{n}(\vec{r}_{\text{s}}) \cdot \vec{\nabla}T(\vec{r}) \Big|_{\vec{r}=\vec{r}_{\text{s}}}. \quad (9)$$

The system of eqn (1)–(6) with the appropriate boundary conditions was solved numerically using the finite element software COMSOL Multiphysics to obtain the self-propulsion speed of the particle, see Section 7.

‡ In general, the nature of the surface boundary condition can be a function of the position on the surface. For example, the coated side of the hot swimmer could be conducting and the uncoated side insulating. We will work under the assumption that the entire surface of the hot swimmer has a single electrostatic boundary condition, unless indicated otherwise, in order to make analytic progress.

3 Linear analytic theory

To gain deeper insight into our system, we derive expressions for the speed of the thermoelectrophoretic swimmer U by linearizing eqn (1)–(6). The approach we employ is similar to that of ref. 38, but applied here also to the temperature dependencies.

Our first linearization is of the electrostatic potential and the ion distributions, *i.e.*, we make the usual Debye–Hückel approximation. § We write

$$n_{\pm}(\vec{r}) = n^{\infty}[1 + x_{\pm}(\vec{r})], \quad (10)$$

$$\Phi(\vec{r}) = \frac{k_{\text{B}}T^{\infty}}{e}\phi(\vec{r}), \quad (11)$$

where $x_{\pm}(\vec{r})$ and $\phi(\vec{r})$ are the dimensionless, linearized ion distributions and potential, respectively.

Our second linearization decomposes the fields and physical quantities into equilibrium (“eq”) and non-equilibrium (“neq”) parts, where the non-equilibrium parts are due to variations in temperature. Here, we shall expand in the small parameter $\tau \equiv \Delta T/T^{\infty}$, corresponding to the relative maximum temperature difference ΔT from the reservoir temperature T^{∞} . Note that τ is well-defined both for the constant temperature boundary condition ($k_{\text{cap}} \ll k_{\text{s}}, k_{\text{f}}$), where we impose the maximum difference, for and the constant heat-flux boundary condition ($k_{\text{cap}} \gg k_{\text{s}}, k_{\text{f}}$), where it needs to be computed, see Appendix B.

This choice of expansion parameter allows us to write to the temperature distribution as

$$T(\vec{r}) = T^{\infty}[1 + \tau t(\vec{r})], \quad (12)$$

where $t(\vec{r})$ is the dimensionless or reduced temperature. Similarly, for the other physical fields the decomposition yields: $x_{\pm}(\vec{r}) = x_{\pm}^{\text{eq}}(\vec{r}) + \tau x_{\pm}^{\text{neq}}(\vec{r})$, $\phi(\vec{r}) = \phi^{\text{eq}}(\vec{r}) + \tau \phi^{\text{neq}}(\vec{r})$, $\vec{u}(\vec{r}) = \tau \vec{v}(\vec{r})$, and $p(\vec{r}) = p^{\text{eq}}(\vec{r}) + \tau p^{\text{neq}}(\vec{r})$. Notice that in equilibrium there is no fluid flow, hence we only have the out-of-equilibrium \vec{v} velocity component. We simplify the equations further by introducing the conjugate variables to the ionic distributions: the local salinity

$$X(\vec{r}) \equiv \frac{x_{+}(\vec{r}) + x_{-}(\vec{r})}{2}, \quad (13)$$

and the local ion excess or space charge density

$$\delta X(\vec{r}) \equiv \frac{x_{+}(\vec{r}) - x_{-}(\vec{r})}{2}. \quad (14)$$

The physical quantities are expanded as: $\varepsilon/\varepsilon^{\infty} = 1 + \tau \varepsilon^* t(\vec{r})$, $\eta/\eta^{\infty} = 1 + \tau \eta^* t(\vec{r})$, $D_{\pm}/D_{\pm}^{\infty} = 1 + \tau D_{\pm}^* t(\vec{r})$, $\alpha_{\pm}/\alpha_{\pm}^{\infty} = 1 + \tau \alpha_{\pm}^* t(\vec{r})$, $k/k^{\infty} = 1 + \tau k^* t(\vec{r})$. Here, the “ ∞ ” superscript

§ It should be noted that in some cases, particularly those involving thermo-charging,^{21,24,36} resorting to the Debye–Hückel approximation is unnecessary. However, in the case of self- and external thermo(di)electrophoresis, the radial symmetry breaking due to the temperature gradient leads to complicated differential equations that only sometimes have closed-form solutions. This will turn out to limit the applicability of our analytic results in the Hückel limit for insulating swimmers, see Section 7.

denotes the reservoir value, which is located at infinity, and the “*” superscript the first-order Taylor expansion coefficient. We have numerically verified that all starred quantities are order unity and that the non-equilibrium fields are much smaller than the equilibrium contributions, see Appendix A.

We now use the above perturbative expressions to expand all equations in terms of τ , keeping only the zeroth-order and first-order terms. The zeroth order gives the equilibrium equations at constant temperature T^{∞} , which are the standard linear Poisson–Boltzmann equations, see Appendix C. The solution of the linear equilibrium problem is $x_{\pm}^{\text{eq}}(\vec{r}) = \mp \phi^{\text{eq}}(\vec{r})$. The first-order equations capture the leading out-of-equilibrium effects.

The heat equation becomes $\nabla^2 t(\vec{r}) = 0$. The temperature profile can be straightforwardly established, because is simply a Laplacian with relatively simple boundary conditions. This equation system can be solved for using decomposition into Legendre–Fourier modes, which respect the rotational symmetry of the problem. The temperature profile for the boundary conditions in which we are interested, was obtained by Bickel *et al.*³¹ under the additional assumption $k_{\text{s}} = k_{\text{f}}$. We therefore do not reproduce their calculation here, but for completeness we provide the relevant expressions in our notation in Appendix B.

The Poisson equation reduces to

$$\nabla^2 \phi^{\text{neq}}(\vec{r}) + \varepsilon^* \vec{\nabla} \cdot (t(\vec{r}) \vec{\nabla} \phi^{\text{eq}}(\vec{r})) = -(\kappa^{\infty})^2 \delta X^{\text{neq}}(\vec{r}), \quad (15)$$

with the inverse reservoir Debye length

$$\kappa^{\infty} \equiv \frac{1}{\lambda^{\infty}} \equiv \sqrt{\frac{2e^2 n^{\infty}}{\varepsilon^{\infty} k_{\text{B}} T^{\infty}}}. \quad (16)$$

The Stokes equations read

$$\begin{aligned} \eta^{\infty} \Delta \vec{v}(\vec{r}) - \vec{\nabla} p^{\text{neq}}(\vec{r}) &= 2k_{\text{B}} T^{\infty} n^{\infty} \left[\delta X^{\text{neq}}(\vec{r}) \vec{\nabla} \phi^{\text{eq}}(\vec{r}) \right. \\ &\quad \left. - \phi^{\text{eq}}(\vec{r}) \vec{\nabla} \phi^{\text{neq}}(\vec{r}) \right. \\ &\quad \left. + \frac{1}{2} (\lambda^{\infty})^2 \varepsilon^* \left| \vec{\nabla} \phi^{\text{eq}}(\vec{r}) \right|^2 \vec{\nabla} t(\vec{r}) \right], \end{aligned} \quad (17)$$

$$\vec{\nabla} \cdot \vec{v}(\vec{r}) = 0, \quad (18)$$

where we used $\partial \varepsilon / \partial T = \varepsilon^{\infty} \varepsilon^* / T^{\infty}$.

Finally, the ionic fluxes become

$$\begin{aligned} \vec{j}_{\pm}^{\text{neq}}(\vec{r}) &= -D_{\pm}^{\infty} n^{\infty} \left[\vec{\nabla} x_{\pm}^{\text{neq}}(\vec{r}) \pm \vec{\nabla} \phi^{\text{neq}}(\vec{r}) \right. \\ &\quad \left. + 2(1 \mp \phi^{\text{eq}}(\vec{r})) \alpha_{\pm}^{\infty} \vec{\nabla} t(\vec{r}) \mp t(\vec{r}) \vec{\nabla} \phi^{\text{eq}}(\vec{r}) \right], \end{aligned} \quad (19)$$

$$\vec{\nabla} \cdot \vec{j}_{\pm}^{\text{neq}}(\vec{r}) = 0, \quad (20)$$

The physical interpretation of eqn (19) is that the flux is generated from left to right by: (i) Diffusion that counters a concentration gradient. (ii) Ion migration in an electric field. (iii) Migration in a temperature gradient through the Soret effect, which has bare migration term and one that couples to the presence of an electric field. (iv) Migration due to temperature

coupling to an electric field, which accounts for the difference in temperature dependence between electric mobility and regular diffusion. Ultimately, point (iv) implies that there can be thermo-electrophoretic swimming without any α_{\pm} -effect, also see ref. 24. From eqn (22) it follows that a non-equilibrium ionic excess will be present even if $\alpha_{\pm} = 0$, in agreement with ref. 22–24.

Remarkably, within the linearized system, only terms involving ε^* introduce the temperature dependence of the physical properties into the equations. That is, no other starred parameters, which indicate the temperature dependence of physical quantities, appear to linear order in τ ! The presence of ε^* is why a thermoelectrophoretic component to this phoresis has been reported in the literature.^{24,34–36,39} The above might be surprising, but it can be readily understood by the fact that, within our expansion, equilibrium and non-equilibrium quantities are always paired. For example, the parameter D_{\pm}^* , which gives the temperature dependence with respect to the reservoir values of the regular diffusion coefficients D_{\pm}^{∞} , is paired with the flux in equilibrium. However, the flux in equilibrium vanishes, hence this term does not appear in eqn (19). Physically speaking, variation of fields with temperature outweighs variation of quantities with temperature, for all but the dielectric coefficient.

We can use the flux eqn (19) to obtain equations for the conjugate variables (13) and (14) by adding and subtracting the two sign variants. Subsequently, we employ the conservation eqn (20) and arrive at

$$\nabla^2 X^{\text{neq}}(\vec{r}) = \beta \vec{\nabla} t(\vec{r}) \cdot \vec{\nabla} \phi^{\text{eq}}(\vec{r}); \quad (21)$$

$$\begin{aligned} \nabla^2 \delta X^{\text{neq}}(\vec{r}) + \nabla^2 \phi^{\text{neq}}(\vec{r}) &= (1 + \gamma) \vec{\nabla} t(\vec{r}) \cdot \vec{\nabla} \phi^{\text{eq}}(\vec{r}) \\ &+ (\kappa^{\infty})^2 t(\vec{r}) \phi^{\text{eq}}(\vec{r}), \end{aligned} \quad (22)$$

where we have used $\nabla^2 t(\vec{r}) = 0$ and introduced

$$\beta \equiv \alpha_+^{\infty} - \alpha_-^{\infty}, \quad (23)$$

$$\gamma \equiv \alpha_+^{\infty} + \alpha_-^{\infty}, \quad (24)$$

with β commonly referred to as the (reduced) Seebeck parameter. This indicates how excess charge is transported in a temperature field, *e.g.*, for $\beta > 0$, the excess charge accumulates in hot regions. The coefficient γ indicates how the background ionic strength is modified by a temperature gradient.

Establishing a solution to the above equation system is nontrivial.¶ Eqn (21) and (22) reveal that the cross coupling between temperature fields and equilibrium ionic screening is crucial to obtain thermoelectrophoresis. If we ignore such cross terms, only the trivial solution is obtained. This intrinsic nonlinearity complicates obtaining solutions using standard

¶ The fields $\delta X^{\text{neq}}(\vec{r})$ and $\phi^{\text{neq}}(\vec{r})$ form a closed subsystem of equations, to linear order in τ . The non-equilibrium ion concentration X^{neq} in eqn (21) is only due to coupling between the temperature gradient and the equilibrium ion potential. It is weighted by the difference in thermal diffusion factors β , meaning that X^{neq} vanishes, when there is no thermal-diffusion-factor-based ion accumulation in the double layer ($\alpha_+^{\infty} = \alpha_-^{\infty} = 0$ or $\alpha_+^{\infty} = \alpha_-^{\infty}$). The closed subsystem is the only non-equilibrium part that then remains. This feature suggests a route toward solving the full set of equations, which is explored in Section 6.

spectral methods.¶ Nevertheless, we stress that the theory is still fully linear in terms of the temperature dependence.

4 The Smoluchowski limit

In this section, we will limit ourselves to the case of high ionic strength and make the thin-screening-layer approximation. We compute the swim speed both using the slip-layer approximation and Teubner's integral formalism³² to double check the expressions and demonstrate it as a valid approach.

4.1 The electrostatic potential and ion profiles

In the high-ionic-strength or Smoluchowski limit, the electrostatic screening length λ^{∞} is small compared to the particle radius, $\kappa^{\infty} a \gg 1$. Outside (“out”) of the screening layer, we have $\nabla^2 X_{\text{out}}^{\text{neq}}(\vec{r}) = 0$ and $\nabla^2 \phi_{\text{out}}^{\text{neq}}(\vec{r}) = 0$, since $\phi^{\text{eq}}(\vec{r}) = 0$ in this region and $\delta X_{\text{out}}^{\text{neq}}(\vec{r}) = 0$, because any excess charge is screened. This implies that the only solutions for the potential and total salinity permissible in the region outside of the double layer have a Laplace form. We know that the temperature satisfies this equation and that it sets up fluxes of ions in the bulk. These fluxes will thus be proportional to the reduced temperature t .

Clearly, in the bulk there cannot be charge separation due to differences in either the regular diffusion coefficients or thermal diffusion factors, otherwise a macroscopic net charge would appear. An unscreened non-equilibrium potential forms in response to any such separation and acts to impose equal effective diffusion. The induced potential is therefore proportional to β in our case. The above mechanism is known as ambipolar diffusion, which in ionic systems results in a state of quasineutrality, *e.g.*, see ref. 38, 40 and 41. Furthermore, ion transport in a thermal gradient can affect the local salinity, as ions may be repelled from or drawn towards areas of higher temperature; this effect scales with γ . Using eqn (19), one indeed finds that $X_{\text{out}}^{\text{neq}}(\vec{r}) = -\gamma t(\vec{r})$ and $\phi_{\text{out}}^{\text{neq}}(\vec{r}) = -\beta t(\vec{r})$, in agreement ref. 21.

Now we turn our attention to the region inside the screening layer, for which we label our fields using the subscript “in”. Let $\lambda^{\infty} q$ measure distance in the direction perpendicular to the surface, with $q = 0$ for $r = a$. In the Smoluchowski approximation, the curvature of the sphere can locally be ignored when describing the region inside the screening layer. We can then split the solutions into parallel and perpendicular components: $\phi^{\text{eq}}(\vec{r}_s, q) = \phi(\vec{r}_s) e^{-q}$ and $t(\vec{r}_s, q) = t(\vec{r}_s)$. Here, $\phi(\vec{r}_s)$ is the potential at the surface and $t(\vec{r}_s)$ is the temperature at the surface. The temperature is approximately radially constant on scales comparable to λ^{∞} because it decays with a power law of

¶ By “nonlinearity” we mean here that the differential equation system cannot be cast into the ‘standard form’ of a Laplacian acting on a vector comprising the individual expansion fields equated to a coefficient matrix acting on the same vector, as was, *e.g.*, done in ref. 38. This hinders a solution strategy based on orthogonalization of this matrix and recovery of the relevant decay lengths as the diagonal elements of the resulting eigenmatrix.

leading order a/r and is therefore much longer ranged than exponential decay.

In this limit, the boundary conditions at the surface of the particle ($q = 0$) need to be determined. N.B. Here, we do not consider temperature-dependent charge regulation. We linearize the conducting and insulating conditions, leading to $\phi_{\text{in}}^{\text{neq}}(\vec{r}_s, 0) = 0$ and $\partial_q \phi_{\text{in}}^{\text{neq}}(\vec{r}_s, q)|_{q=0} = 0$, respectively. For a conductor, the equilibrium part of the field accounts fully for the surface potential, $\phi_{\text{in}}^{\text{eq}}(\vec{r}_s, 0) = \phi_0(\vec{r}_s)$, with $\phi_0(\vec{r}_s)$ the reduced surface potential. This implies $\phi_{\text{in}}^{\text{eq}}(\vec{r}_s, q) = \phi_0(\vec{r}_s)e^{-q}$. For an insulator, the boundary condition of the equilibrium potential

$$\partial_q \phi_{\text{in}}^{\text{eq}}(\vec{r}_s, q)|_{q=0} = -\frac{\lambda^\infty e \sigma(\vec{r}_s)}{\varepsilon^\infty k_B T^\infty}, \quad (25)$$

covers any surface charge present. This implies that

$$\phi_{\text{in}}^{\text{eq}}(\vec{r}_s, q) = \frac{\lambda^\infty e}{\varepsilon^\infty k_B T^\infty} \sigma(\vec{r}_s) e^{-q}, \quad (26)$$

which matches a series expansion of the full solution for the curved surface in terms of $\lambda^\infty \ll a$. Note that throughout this section, the electrostatic boundary condition could, in principle, vary along the surface, only in the next section we will make a further reduction and assume it is homogeneous.

Considering the above, it is possible to write in general $\phi_{\text{in}}^{\text{eq}}(\vec{r}_s, q) = \phi(\vec{r}_s)e^{-q}$, with $\phi(\vec{r}_s)$ either $\phi_0(\vec{r}_s)$ (conducting) or equal to the prefactor in eqn (26) (insulating). The fact that the insulating case has a prefactor λ^∞ does not have consequences for the expansions that will be performed next, as the parallel components scale $\mathcal{O}(1)$, and all other components either $\mathcal{O}(\kappa^\infty)$ or $\mathcal{O}((\kappa^\infty)^2)$. However, as we will see in Section 7.6, it will have consequences for the speeds that can be achieved in the Smoluchowski limit by an insulating swimmer.

Applying the coordinate transformation inside the screening layer, we have for the Laplacian: $\nabla^2 = \nabla_{\parallel}^2 + (\kappa^\infty)^2 \partial_q^2$, with $\vec{\nabla}_{\parallel}$ the gradient in the tangent plane to \vec{r}_s and ∇_{\parallel}^2 the associated in-plane Laplacian. Taking the limit $\lambda^\infty \downarrow 0$, leads to the following transformed salinity and space charge density

$$\partial_q^2 X_{\text{in}}^{\text{neq}}(\vec{r}_s, q) = 0; \quad (27)$$

$$\partial_q^2 \delta X_{\text{in}}^{\text{neq}}(\vec{r}_s, q) + \partial_q^2 \phi_{\text{in}}^{\text{neq}}(\vec{r}_s, q) = t(\vec{r}_s) \phi(\vec{r}_s) e^{-q}, \quad (28)$$

with corresponding Poisson equation

$$\partial_q^2 \phi_{\text{in}}^{\text{neq}}(\vec{r}_s, q) = -\varepsilon^* t(\vec{r}_s) \phi(\vec{r}_s) e^{-q} - \delta X_{\text{in}}^{\text{neq}}(\vec{r}_s, q). \quad (29)$$

Since only derivatives with respect to q remain in eqn (27)–(29), they can be solved using separation of variables.

The limit $|\vec{r}| \downarrow a$ for the solutions outside of the screening layer gives a set of boundary conditions for the solution inside. Note that by construction this corresponds to $q \uparrow \infty$. Taking this limit within the layer, we obtain the conditions $X_{\text{in}}^{\text{neq}}(\vec{r}_s, q \uparrow \infty) = -\gamma t(\vec{r}_s)$, $\delta X_{\text{in}}^{\text{neq}}(\vec{r}_s, q \uparrow \infty) = 0$, and $\phi_{\text{in}}^{\text{neq}}(\vec{r}_s, q \uparrow \infty) = -\beta t(\vec{r}_s)$. The right-hand value is evaluated at the edge of the screening layer $\vec{r}_s^+ \approx \vec{r}_s$, in order to avoid the ambiguity that arises by simultaneously demanding $\lambda^\infty \downarrow 0$.

The above conditions, together with the linearized eqn (27)–(29), lead to the following solutions within the screening layer.

The non-equilibrium space charge density decays with q , and we must consider conducting (equipotential) and insulating (fixed charge) surfaces separately, in all cases.

We start with the solution for the total space charge density. The temperature decays very little inside the screening layer, therefore the added total salinity due to the heating therein is given by $X_{\text{in}}^{\text{neq}}(\vec{r}_s, q) = -\gamma t(\vec{r}_s)$. However, the modification of the net salt concentration in the double layer is sufficiently small that local corrections to the Debye length do not have to be accounted for, since $X_{\text{in}} = X_{\text{in}}^{\text{eq}} + \tau X_{\text{in}}^{\text{neq}}$ with $\tau \ll 1$.

Next, we provide the results for the out-of-equilibrium part of the local ion excess and electrostatic potential. For an equipotential surface (or conductor), we find

$$\delta X_{\text{in}}^{\text{neq}}(\vec{r}_s, q) = -\beta t(\vec{r}_s) e^{-q} + \frac{1}{2} \phi(\vec{r}_s) t(\vec{r}_s) [2 - (1 + \varepsilon^*)q] e^{-q}, \quad (30)$$

where the electrostatic potential is given by

$$\begin{aligned} \phi_{\text{in}}^{\text{neq}}(\vec{r}_s, q) &= -\beta t(\vec{r}_s) (1 - e^{-q}) \\ &+ \frac{1}{2} \phi(\vec{r}_s) t(\vec{r}_s) [(1 + \varepsilon^*)q] e^{-q}, \end{aligned} \quad (31)$$

because $\phi_{\text{in}}^{\text{neq}}(\vec{r}_s, 0) = 0$. For a fixed, homogeneous surface charge, we find

$$\delta X_{\text{in}}^{\text{neq}}(\vec{r}_s, q) = \frac{1}{2} \phi(\vec{r}_s) t(\vec{r}_s) [2 - (1 + \varepsilon^*)(1 + q)] e^{-q}, \quad (32)$$

where the associated electrostatic potential reads

$$\phi_{\text{in}}^{\text{neq}}(\vec{r}_s, q) = -\beta t(\vec{r}_s) + \frac{1}{2} \phi(\vec{r}_s) t(\vec{r}_s) [(1 + \varepsilon^*)(1 + q)] e^{-q}. \quad (33)$$

In both cases the Seebeck effect thus leads to the development of a surface thermocharge, which is given by $\delta X_{\text{in}}^{\text{neq}} = (\phi_0 - \beta)t$ for a conductor** and the $q \downarrow 0$ variant of eqn (32) for an insulator.†† These expressions differ from the ones found by Majee and Würger²¹ in that we include a non-zero imposed surface potential. Moreover, by the surface thermocharge, we mean the charge that is imposed directly at the surface, rather than the integral form that is employed in ref. 21 and 24, which gives the effective bulk thermocharge around the swimmer due to thermophoresis.

4.2 Thermo(di)electrophoretic force onto the fluid

We must first determine the forces acting on the fluid to perform the slip-layer approximation and obtain the swim speed. The equilibrium component of the force only generates a hydrostatic pressure, which cannot contribute to the generation of flow, by definition, see Appendix C. For analytic convenience,

** The charging for $\beta = 0$ follows from the right-hand side of eqn (28). Suppose for convenience that $\varepsilon^* = 0$ then eqn (28) and (29) combine to give an inhomogeneous Helmholtz equation for $\delta X_{\text{in}}^{\text{neq}}$, for which the particular solution exactly corresponds to minus the right-hand side of eqn (28). Physically, the effect is due to the difference in temperature dependence between regular diffusion and electric migration,^{22,23} which gives an additional contribution to surface (and bulk) thermocharge on top of that induced by the Seebeck effect.^{21,24}

†† Here too, there is a thermocharging effect ($\delta X_{\text{in}}^{\text{neq}}(\vec{r}_s, q) \neq 0$) as described in ref. 21 and 24. However, there is only a non-Seebeck contribution, which means that uncharged surfaces cannot pick up a surface thermocharge. They can pick up a bulk thermocharge, as follows from using the definition in ref. 21 and 24. In general, we will restrict our analysis to the case $\phi(\vec{r}_s) \neq 0$.

we will assume that the reduced surface potential $\phi(\vec{r}_s)$ is locally uniform, *i.e.*, $\vec{\nabla}_{\parallel}\phi(\vec{r}_s) = \vec{0}$. We use the general form of the Stokes equation $\eta^{\infty}\underline{\Delta}\vec{v} = \vec{\nabla}p^{\text{neq}} - \vec{f}^{\text{neq}}$ to identify the out-of-equilibrium force density acting on the fluid in a first-order expansion

$$\frac{\vec{f}^{\text{neq}}(\vec{r})}{k_{\text{B}}T^{\infty}n^{\infty}} = -2\delta X^{\text{neq}}(\vec{r})\vec{\nabla}\phi^{\text{eq}}(\vec{r}) + 2\phi^{\text{eq}}(\vec{r})\vec{\nabla}\phi^{\text{neq}}(\vec{r}) - (\lambda^{\infty})^2\varepsilon^* \left| \vec{\nabla}\phi^{\text{eq}}(\vec{r}) \right|^2 \vec{\nabla}t(\vec{r}). \quad (34)$$

Outside the screening layer, the force density vanishes $\ddagger\ddagger$

$$\frac{\vec{f}_{\text{out}}^{\text{neq}}(\vec{r})}{k_{\text{B}}T^{\infty}n^{\infty}} = \vec{0}. \quad (35)$$

Inside of the screening layer, we can split the driving forces into components parallel and perpendicular to the surface. These read

$$\frac{\vec{f}_{\text{in},\parallel}^{\text{neq}}(\vec{r}_s, q)}{k_{\text{B}}T^{\infty}n^{\infty}} = 2\phi(\vec{r}_s)e^{-q}\vec{\nabla}_{\parallel}\phi^{\text{neq}}(\vec{r}_s, q) - \varepsilon^*\phi(\vec{r}_s)^2e^{-2q}\vec{\nabla}_{\parallel}t(\vec{r}_s); \quad (36)$$

$$\frac{\vec{f}_{\text{in},\perp}^{\text{neq}}(\vec{r}_s, q)}{k_{\text{B}}T^{\infty}n^{\infty}} = 2\kappa^{\infty}\phi(\vec{r}_s)e^{-q}[\delta X^{\text{neq}}(\vec{r}_s, q) + \partial_q\phi^{\text{neq}}(\vec{r}_s, q)]\hat{q}, \quad (37)$$

where we have used that $t(\vec{r})$ is almost constant in the perpendicular direction over the length of the double layer, as we did previously in Section 4.1. We have also introduced the unit normal to the sphere's surface \hat{q} , which points outward.

The expressions for the force density inside the screening layer can be rewritten using the expressions for the density and potential. For the perpendicular component we find

$$\frac{\vec{f}_{\text{in},\perp}^{\text{neq}}(\vec{r}_s, q)}{k_{\text{B}}T^{\infty}n^{\infty}} = -\kappa^{\infty}[4\beta - (3 + \varepsilon^* - 2(1 + \varepsilon^*)q)\phi(\vec{r}_s)] \times \phi(\vec{r}_s)e^{-2q}t(\vec{r}_s)\hat{q}, \quad (38)$$

which holds for the equipotential surface, and

$$\frac{\vec{f}_{\text{in},\perp}^{\text{neq}}(\vec{r}_s, q)}{k_{\text{B}}T^{\infty}n^{\infty}} = \kappa^{\infty}[1 - \varepsilon^* - 2(1 + \varepsilon^*)q]\phi(\vec{r}_s)^2e^{-2q}t(\vec{r}_s)\hat{q}, \quad (39)$$

which holds for insulating surface. Under the same assumption, we obtain

$$\frac{\vec{f}_{\text{in},\parallel}^{\text{neq}}(\vec{r}_s, q)}{k_{\text{B}}T^{\infty}n^{\infty}} = -[2(1 - e^{-q})\beta + (\varepsilon^* - (1 + \varepsilon^*)q)\phi(\vec{r}_s)e^{-q}] \times \phi(\vec{r}_s)e^{-q}\vec{\nabla}_{\parallel}t(\vec{r}_s); \quad (40)$$

$\ddagger\ddagger$ Higher-order terms would lead to a force in the bulk, however this contribution is small, scaling with τ^3 , and is therefore ignored here. That is, there is an unscreened electric field ($\phi_{\text{out}}^{\text{neq}}(\vec{r}) = -\beta t(\vec{r})$) and a temperature gradient in the bulk. The latter would lead to a temperature-variation of the dielectric permittivity, while the former ensures that the potential prefactor in the permittivity term of eqn (5) is nonzero. Hence there will be a force contribution in the bulk even with strong screening.

$$\frac{\vec{f}_{\text{in},\parallel}^{\text{neq}}(\vec{r}_s, q)}{k_{\text{B}}T^{\infty}n^{\infty}} = -[2\beta - (1 + (1 + \varepsilon^*)q)\phi(\vec{r}_s)e^{-q}]\phi(\vec{r}_s)e^{-q}\vec{\nabla}_{\parallel}t(\vec{r}_s), \quad (41)$$

for the equipotential and insulating surface, respectively.

4.3 The slip-layer approximation

At this point of the calculation, we make the slip-layer approximation. We have already assumed a high ionic strength and therefore all the thermoelectrophoretic speed is generated in a small layer around the colloid. This implies that no-slip boundary condition on the colloid may be replaced by an effective slip/velocity boundary that accounts for the speed generation in the thin Debye layer, *e.g.*, see ref. 42–44.

Decomposing the Stokes equations into parallel and perpendicular components, we obtain the following expressions:

$$\eta^{\infty}(\kappa^{\infty})^2\partial_q^2\vec{v}_{\parallel}(\vec{r}_s, q) = \vec{\nabla}_{\parallel}p^{\text{neq}}(\vec{r}_s, q) - \vec{f}_{\text{in},\parallel}^{\text{neq}}(\vec{r}_s, q); \quad (42)$$

$$\kappa^{\infty}\hat{q}\partial_q p^{\text{neq}}(\vec{r}_s, q) = f_{\text{in},\perp}^{\text{neq}}(\vec{r}_s, q), \quad (43)$$

where in eqn (42) the decomposed Laplacian acts only on the parallel velocity components and only the double derivative with respect to q remains; it dominates due to the $(\kappa^{\infty})^2$ prefactor. In eqn (43), we used that the perpendicular fluid velocity (*i.e.*, toward the particle) in the thin layer must be zero, due to incompressibility of the fluid.

Solving for the q -dependence of the pressure using eqn (43), we find the following expressions

$$\frac{p^{\text{neq}}(\vec{r}_s, q)}{k_{\text{B}}T^{\infty}n^{\infty}} = [2\beta - (1 - (1 + \varepsilon^*)q)\phi(\vec{r}_s)]\phi(\vec{r}_s)t(\vec{r}_s)e^{-2q}; \quad (44)$$

$$\frac{p^{\text{neq}}(\vec{r}_s, q)}{k_{\text{B}}T^{\infty}n^{\infty}} = [\varepsilon^* + (1 - (1 + \varepsilon^*)q)]\phi(\vec{r}_s)^2t(\vec{r}_s)e^{-2q}, \quad (45)$$

for conducting and insulating surfaces, respectively. Here, we have set the non-equilibrium pressure to zero for ($q \uparrow 0$), because the equilibrium component is subtracted in our linearization.

One can group the parallel pressure gradient and parallel force terms in eqn (42) and solve the resulting differential equation for $\vec{v}_{\parallel}(\vec{r}_s, q)$, with boundary condition $v_{\parallel}(\vec{r}_s, q \downarrow 0) = \vec{0}$. The slip speed may be obtained by taking the limit $\vec{v}_{\text{slip}}(\vec{r}_s) = \lim_{q \rightarrow \infty} \vec{v}_{\parallel}(\vec{r}_s, q)$ and it is given by

$$\vec{v}_{\text{slip}}(\vec{r}_s) = \frac{(\lambda^{\infty})^2}{4\eta^{\infty}}k_{\text{B}}T^{\infty}n^{\infty}[8\beta - (1 - \varepsilon^*)\phi(\vec{r}_s)]\phi(\vec{r}_s)\vec{\nabla}_{\parallel}t(\vec{r}_s). \quad (46)$$

The above result is quite surprising, as the slip velocity has the same functional form for both insulating and conducting surfaces, as was also reported in ref. 24.

The speed of the particle is now obtained by evaluating the integral

$$\bar{U} = -\frac{1}{4\pi a^2} \oint \vec{v}_{\text{slip}} d\vec{r}_s. \quad (47)$$

where \vec{v}_{slip} is the slip velocity and integration takes place over the particle's surface. We obtain for the total speed of a swimmer

$$\bar{U} = -\frac{k_{\text{B}}T^{\infty}n^{\infty}}{6\eta^{\infty}a}(\lambda^{\infty})^2 \left[8\beta\phi(\vec{r}_s) - (1 - \varepsilon^*)\phi(\vec{r}_s)^2 \right] \bar{t}_1, \quad (48)$$

to leading order in λ^{∞} . Here, \bar{t}_1 is the first Legendre–Fourier coefficient in a decomposition of the temperature, see Appendix B.

4.4 The speed according to Teubner

We verify the slip-layer swim speed by employing Teubner's method³² of integrating the (out-of-equilibrium) body force density with an integration kernel $\underline{K}(\vec{r})$ to obtain the reduced swim speed

$$\bar{U} = \frac{1}{6\pi\eta^{\infty}a} \int_V \underline{K}(\vec{r}) \cdot \vec{f}^{\text{neq}}(\vec{r}) d\vec{r}; \quad (49)$$

$$\underline{K}(\vec{r}) = \left(\frac{3a}{2r} - \frac{a^3}{2r^3} - 1 \right) \cos\theta\hat{r} - \left(\frac{3a}{4r} + \frac{a^3}{4r^3} - 1 \right) \sin\theta\hat{\theta}, \quad (50)$$

where integration takes place over the volume V outside of the particle. The laborious calculation of the swim speed *via* this route is provided in Appendix D. Grouping the expressions therein together, we obtain for the speed exactly the result of eqn (48).

5 The Hückel limit

In this section, we use a regime-splitting approach to determine the leading-order departure from the salt-free limit. That is, we study systems in which the Debye length is large $\kappa^{\infty}a \ll 1$.

5.1 Splitting the equation system

We start from the equations for the equilibrium and non-equilibrium fields, of which the former are provided in Appendix C and the latter are given by eqn (15), (21) and (22). The equilibrium electric field obeys the regular Debye–Hückel expression

$$\phi^{\text{eq}}(\vec{r}) = \phi_s \left(\frac{a}{r} \right) e^{-\kappa^{\infty}(r-a)}, \quad (51)$$

where ϕ_s is a homogeneous surface potential, related either to the conducting or the insulating boundary condition.

We introduce the splitting parameter $\xi = \kappa^{\infty}a \ll 1$ and the coordinate transform $\vec{r} \equiv a\vec{y}$ to approximate the equilibrium potential as

$$\phi^{\text{eq}}(\vec{y}) = \begin{cases} \tilde{\phi}_s/y & y < \xi^{-1} \\ 0 & y > \xi^{-1} \end{cases}, \quad (52)$$

§§ This integration kernel isolates *via* projection those components of the body force that contribute to the speed of the particle, from those that create higher-order (multipolar) flow fields that do not contribute to locomotion. That is, the entries in the kernel have the same decay as found for fluid velocity around a dragged sphere. Note that our integral is thus also reminiscent some of the steps taken in the reciprocal approach recently proposed by Burelbach and Stark.²⁵

up to order $\mathcal{O}(1)$. The physical reasoning behind this approach is that for very large screening layers, the potential is essentially unscreened for a sizable fraction of the very large Debye length. However, outside of the screening layer, it must still vanish. Eqn (52) gives an approximate form to this intuition. Above, we have introduced the expansion prefactor $\tilde{\phi}_s$, which assumes the value $\tilde{\phi}_s = \phi_0$ for a conductor and $\tilde{\phi}_s = (ae\sigma_0)/(k_{\text{B}}T^{\infty}\varepsilon^{\infty})$ for an insulator, respectively. Note that we assume that the potential is essentially unscreened inside the double layer and fully screened outside; we still require $x_{\pm}(\vec{y}) = \mp\phi^{\text{eq}}(\vec{y})$.

Using the above expressions and expanding eqn (15), (21) and (22) to $\mathcal{O}(\xi)$, we obtain the following for $y < \xi^{-1}$:

$$\nabla^2\phi_{\text{in}}^{\text{neq}}(\vec{y}) = -\varepsilon^*\vec{\nabla}t(\vec{y}) \cdot \vec{\nabla}\phi^{\text{eq}}(\vec{y}); \quad (53)$$

$$\nabla^2X_{\text{in}}^{\text{neq}}(\vec{y}) = \beta\vec{\nabla}t(\vec{y}) \cdot \vec{\nabla}\phi^{\text{eq}}(\vec{y}); \quad (54)$$

$$\nabla^2\delta X_{\text{in}}^{\text{neq}}(\vec{y}) = (1 + \gamma + \varepsilon^*)\vec{\nabla}t(\vec{y}) \cdot \vec{\nabla}\phi^{\text{eq}}(\vec{y}). \quad (55)$$

The relation $a\vec{\nabla}_{\vec{r}} = \vec{\nabla}_{\vec{y}}$ was used to obtain gradients and Laplacians in terms of \vec{y} ; the subscript is dropped throughout for notational convenience. Note that the equations for all fields have the same shape, which can be solved for, see Appendix E.

5.2 The thermo(di)electrophoretic body force

Employing the general solution, eqn (101) from Appendix E, we obtain solutions to eqn (53)–(55) by imposing boundary conditions. We start with $\phi_{\text{in}}^{\text{neq}}$, which vanishes at the surface of the particle for an equipotential surface, leading to

$$\phi_{\text{in}}^{\text{neq}}(\vec{y}) = \frac{1}{2} \sum_{j=0}^{\infty} \check{t}_j \psi_j(y) P_j(\cos\theta); \quad (56)$$

$$\psi_j(y) = \varepsilon^* \tilde{\phi}_s (y-1) y^{-(j+2)},$$

where the \check{t}_j are expansion factors related to the temperature distribution, see Appendix E. For an insulating surface, the derivative of $\phi_{\text{in}}^{\text{neq}}$ vanishes at the surface. This leads to the following non-equilibrium potential expansion coefficients

$$\psi_j(y) = -\varepsilon^* \tilde{\phi}_s \frac{(j+1) - (j+2)y}{(j+1)} y^{-(j+2)}. \quad (57)$$

The fields $X_{\text{in}}^{\text{neq}}$ and $\delta X_{\text{in}}^{\text{neq}}(\vec{y})$ are solved for by matching the expansion to the outer boundaries at $|\vec{y}| = \xi^{-1}$, as expressed by $X_{\text{in}}^{\text{neq}}(\vec{y})|_{y=\xi^{-1}} = -\gamma t(y)|_{y=\xi^{-1}}$, and $\delta X_{\text{in}}^{\text{neq}}(\vec{y})|_{y=\xi^{-1}} = -\beta t(y)|_{y=\xi^{-1}}$. This results in

$$X_{\text{in}}^{\text{neq}}(\vec{y}) = -\frac{1}{2} \sum_{j=0}^{\infty} \check{t}_j X_j(y) P_j(\cos\theta); \quad (58)$$

$$X_j(y) = \left[2\gamma y + \beta \tilde{\phi}_s (\xi y - 1) \right] y^{-(j+2)},$$

and

$$\delta X_{\text{in}}^{\text{neq}}(\vec{y}) = -\frac{1}{2} \sum_{j=0}^{\infty} \check{t}_j \delta X_j(y) P_j(\cos\theta); \quad (59)$$

$$\delta X_j(y) = \left[2\beta y + (1 + \gamma + \varepsilon^*) \tilde{\phi}_s (\xi y - 1) \right] y^{-(j+2)},$$

for the non-equilibrium ionic strength and excess charge, respectively. Note that these are the same for insulators and conductors in the splitting formalism.

Outside the double layer ($y > \xi^{-1}$) we have $\phi_{\text{out}}^{\text{neq}}(\vec{y}) = -\beta t(\vec{y})$, $X_{\text{in}}^{\text{neq}}(\vec{y}) = -\gamma t(\vec{y})$, and $\delta X_{\text{in}}^{\text{neq}}(\vec{y}) = 0$, as before. This leads to a vanishing force acting on the fluid up to $\mathcal{O}(\tau^3)$. Inside the screening layer, we write the force on the fluid in terms of \vec{y} and ξ

$$\begin{aligned} \vec{f}_{\text{in}}^{\text{neq}}(\vec{y}) = & -\frac{\varepsilon^\infty (k_{\text{B}} T^\infty)^2}{e^2 a^3} \left[\xi^2 \delta X_{\text{in}}^{\text{neq}}(\vec{y}) \vec{\nabla} \phi_{\text{in}}^{\text{eq}}(\vec{y}) \right. \\ & - \xi^2 \phi_{\text{in}}^{\text{eq}}(\vec{y}) \vec{\nabla} \phi_{\text{in}}^{\text{neq}}(\vec{y}) \\ & \left. + \frac{1}{2} \varepsilon^* \left| \vec{\nabla} \phi_{\text{in}}^{\text{eq}}(\vec{x}) \right|^2 \vec{\nabla} t(\vec{s}) \right]. \end{aligned} \quad (60)$$

Here, the temperature variation of the dielectric permittivity, as specified to first order by ε^* , becomes the dominant term. This is expected, since thermodielectrophoresis is the only effect contributing to the self-propulsion in the salt-free limit (without counterions) and results in a finite swim speed.

5.3 Swim speed in the Hückel limit

The solutions for the fields can be used in conjunction with Teubner's formalism, see eqn (49), to obtain self-propulsion speeds in the Hückel limit; admittedly, after (further) laborious algebraic bookkeeping. The conducting swimmer has a speed

$$\begin{aligned} \tilde{U} = & -\frac{\varepsilon^\infty \varepsilon^* (k_{\text{B}} T^\infty)^2}{105 \eta^\infty e^2 a} \phi_0^2 \tilde{t}_1 \\ & - n^\infty \frac{a k_{\text{B}} T^\infty}{180 \eta^\infty} [30\beta - (4 + 4\gamma + 15\varepsilon^*) \phi_0] \phi_0 \tilde{t}_1, \end{aligned} \quad (61)$$

while that of the insulating swimmer is given by

$$\begin{aligned} \tilde{U} = & -\frac{\varepsilon^\infty \varepsilon^* (k_{\text{B}} T^\infty)^2}{105 \eta^\infty e^2 a} \tilde{\phi}_s^2 \tilde{t}_1 \\ & - n^\infty \frac{a k_{\text{B}} T^\infty}{360 \eta^\infty} [60\beta - (8 + 8\gamma + 45\varepsilon^*) \tilde{\phi}_s] \tilde{\phi}_s \tilde{t}_1, \end{aligned} \quad (62)$$

with $\tilde{\phi}_s = (ae\sigma_0)/(k_{\text{B}} T^\infty \varepsilon^\infty)$. Note that here we have expanded the result in ξ , only retaining terms up to $\mathcal{O}(\xi^3)$, and we have used $\tilde{t}_1 = \tilde{t}_1$. The identity holds for $j = 1$, but conversion factors are generally expected, *i.e.*, $\tilde{t}_{j>1} \neq \tilde{t}_{j>1}$ usually; these terms fortuitously do not contribute to the speed.

From the above speed equations, it is clear that even in the absence of salt, a polarization-based contribution to the swim speed remains. Burelbach and Stark similarly report a constant value of the speed for external thermoelectrophoresis in the Hückel limit,²⁵ which they refer to as a ‘‘colloid hydration’’ term. In addition, the direction of self-propulsion can change with ionic strength. Considering, for example the conducting swimmer, the leading term in the Hückel limit $\tilde{U} \propto -[30\beta - (4 + 4\gamma)\phi_0]\phi_0$ may be smaller than zero ($\varepsilon^* = 0$), whenever the leading term in the Smoluchowski limit $\tilde{U} \propto -[8\beta - \phi_0]\phi_0$ is larger than zero and *vice versa*, depending on the values of β and γ . Lastly, whenever, $\varepsilon^* = 0$, the limiting behavior at low salt concentration is that of a vanishing speed for both electrostatic boundary conditions.

This is not the same as the dependency reported in ref. 25. The difference can be attributed to the geometry of the temperature field, which is not identical between self- and external thermoelectrophoresis in the Hückel limit. Such geometric differences were recently showcased for regular electrophoresis in ref. 38.

6 Intermediate ionic strengths

Now that we have examined the swim speed in both limits of thin and thick screening layers, we can consider what happens in the intermediate regime. The algebra is rather complicated between the two limiting cases, hence we refer to our ESI† for the full details. The main idea is to not only assume a uniform electrostatic boundary condition, but also a specific form for the temperature profile. Only the first mode of the temperature expansion contributes to the speed. Thus, we restrict ourselves to the following temperature distribution $t(r, \theta) = -(a/r)^2 \cos \theta$, where we introduce the minus sign to have a the capping material be on the $z < 0$ hemisphere of the swimmer whenever $\Delta T > 0$.

The relevant cross-coupling terms in eqn (15), (21) and (22) may now be written as

$$t(r) \phi^{\text{eq}}(\vec{r}) = \tilde{C}_0 \cos \theta \left(\frac{a^3}{r^3} \right) e^{-\kappa^\infty r}; \quad (63)$$

$$\vec{\nabla} t(\vec{r}) \cdot \vec{\nabla} \phi^{\text{eq}}(\vec{r}) = 2\tilde{C}_0 [1 + \kappa^\infty r] \cos \theta \left(\frac{a^3}{r^5} \right) e^{-\kappa^\infty r}, \quad (64)$$

where \tilde{C}_0 is a coefficient that accounts for all electrostatic prefactors – both for the equipotential and constant surface charge case – and we have made use of the uniformity of the imposed electrostatic boundary condition. The Poisson eqn (15) reads

$$\begin{aligned} \nabla^2 \phi^{\text{neq}}(\vec{r}) + (\kappa^\infty)^2 \delta X^{\text{neq}}(\vec{r}) = & -\varepsilon^* \tilde{C}_0 \left[2 + 2\kappa^\infty r + (\kappa^\infty r)^2 \right] \\ & \times \cos \theta \left(\frac{a^3}{r^5} \right) e^{-\kappa^\infty r}, \end{aligned} \quad (65)$$

for the local salinity (21) we find

$$\nabla^2 X^{\text{neq}}(\vec{r}) = 2\beta \tilde{C}_0 [1 + \kappa^\infty r] \cos \theta \left(\frac{a^3}{r^5} \right) e^{-\kappa^\infty r}, \quad (66)$$

and for the local charge excess (22) we obtain

$$\begin{aligned} \nabla^2 \delta X^{\text{neq}}(\vec{r}) + \nabla^2 \phi^{\text{neq}}(\vec{r}) = & \tilde{C}_0 \left[2(1 + \gamma) + 2(1 + \gamma)\kappa^\infty r + (\kappa^\infty r)^2 \right] \\ & \times \cos \theta \left(\frac{a^3}{r^5} \right) e^{-\kappa^\infty r}. \end{aligned} \quad (67)$$

Using eqn (65), we obtain a differential equation in terms of $\delta X^{\text{neq}}(\vec{r})$ only, which is given by

$$\begin{aligned} & \nabla^2 \delta X^{\text{neq}}(\vec{r}) - (\kappa^\infty)^2 \delta X^{\text{neq}}(\vec{r}) \\ &= \tilde{C}_0 \left[2(1 + \gamma + \varepsilon^*) + 2(1 + \gamma + \varepsilon^*) \kappa^\infty r + (1 + \varepsilon^*) (\kappa^\infty r)^2 \right] \\ & \times \cos \theta \left(\frac{a^3}{r^5} \right) e^{-\kappa^\infty r}. \end{aligned} \quad (68)$$

We have reduced the problem to an inhomogeneous Laplace equation for local non-equilibrium salinity $X^{\text{neq}}(\vec{r})$, an inhomogeneous Helmholtz equation for the non-equilibrium charge excess $\delta X^{\text{neq}}(\vec{r})$, and another inhomogeneous Laplace equation for the associated non-equilibrium potential $\phi^{\text{neq}}(\vec{r})$; provided that a solution for $\delta X^{\text{neq}}(\vec{r})$ has been established. This system of equations may be solved analytically, although no closed-form expressions can be obtained, see ESI.†

Taking the Smoluchowski limit, we arrive at $\lim_{\kappa \rightarrow 10} \bar{U} = 0$ for the insulating surface and

$$\bar{U} = -\frac{(k_B T^\infty)^2 \varepsilon^\infty}{12e^2 \eta^\infty a} [8\beta \phi_0 - (1 - \varepsilon^*) \phi_0^2], \quad (69)$$

both of which are in agreement with eqn (48). Unfortunately, using the full analytic approach makes it difficult to establish how the speed departs from these limits, see the ESI.† The reason is that expressions appear in the solution that are problematic to evaluate numerically, as they involve the near cancellation of large terms, which gives rise to a small, yet relevant values. This hinders progress *via* a series expansion around the limit.

In the opposite (Hückel) limit, we obtain for a conducting swimmer the following speed

$$\begin{aligned} \tilde{U} &= -\frac{\varepsilon^\infty \varepsilon^* (k_B T^\infty)^2}{105 \eta^\infty e^2 a} \phi_0^2 - \frac{2\varepsilon^\infty \varepsilon^* (k_B T^\infty)^2}{105 \eta^\infty e^2} \kappa^\infty \phi_0^2 \\ & - n^\infty \frac{ak_B T^\infty}{2520 \eta^\infty} (420\beta - (49 - 161\gamma - 16\varepsilon^*) \phi_0) \phi_0. \end{aligned} \quad (70)$$

This expression has a similar shape as eqn (61), barring a $\kappa^\infty \propto \sqrt{n^\infty}$ dependent term. This term comes from the outer region of the solution, where we had assumed a fully screened potential and set the force density to zero in Section 5. We conclude that splitting gives an impression of the limit and some aspects of the departure therefrom, but can lead to qualitatively incorrect scaling. Nonetheless, when $\varepsilon^* = 0$, eqn (61) and (70) agree semi-quantitatively, with only minor changes in the prefactors. Therefore, the method can have merit whenever there is no contribution to self-propulsion outside the screening layer.

The insulating swimmer's speed in the Hückel limit is given by

$$\begin{aligned} \tilde{U} &= -\frac{a\varepsilon^*}{105 \eta^\infty \varepsilon^\infty} \sigma_0^2 - \frac{a^3 e^2}{360 k_B T^\infty \eta^\infty (\varepsilon^\infty)^2} (7 - 23\gamma) n^\infty \sigma_0^2 \\ & - \frac{a^2 e}{6 \eta^\infty \varepsilon^\infty} n^\infty \sigma_0^2 + \frac{8a^3 e^2 \varepsilon^*}{315 k_B T^\infty \eta^\infty (\varepsilon^\infty)^2} n^\infty \sigma_0^2. \end{aligned} \quad (71)$$

This expression also differs from the one provided in Section 5.3 for the same reasons. We will show next that the speeds reported in this section do capture many of the speed features obtained using FEM, despite the limitations of the method.

7 Numerical results

In this section, we discuss our numerical FEM results and show that these correspond to the expressions of our analytic calculations in the appropriate limits. We will predominantly use dimensionful units to make the connection with experiments and to highlight those regimes wherein we expect measurable results.

7.1 Parameter choices

Throughout, we assume a colloidal particle diameter of 1 μm . We consider three types of swimmer material for the hot swimmers: no thermal conductivity contrast with water $K = 1$; polystyrene (PS), $K_{\text{PS}} \equiv k_{\text{PS}}/k_{\text{f}} = 0.0847$; and silica (SiO_2) $K_{\text{SiO}_2} = 2.34$. For the fluid, we use the physical properties of water at $T^\infty = 298.15 \text{ K}$ (room temperature): $\varepsilon^\infty = \varepsilon_0 \varepsilon_{\text{r}}$ with ε_0 the vacuum and $\varepsilon_{\text{r}} = 78.4$ the relative permittivity, $\eta^\infty = 8.9 \times 10^{-4} \text{ Pa s}$, and $k^\infty = k_{\text{f}} = 0.591 \text{ W m}^{-1} \text{ K}^{-1}$.⁴⁵ The ambient pressure is specified to be $p^\infty = 1 \times 10^5 \text{ Pa}$, approximately one atmosphere.

We further consider three types of ions to determine the effect of thermoelectrophoresis, one cation, sodium Na^+ , and two anions, chloride Cl^- and hydroxide OH^- . This choice is based on the commonplaceness of these ions, as well as the fact that the Cl^- anion has a much smaller Soret coefficient than OH^- , allowing us to probe the effect thereof on the motion of the swimmer. The ionic diffusion coefficients are $D_{\text{Na}^+} = 1.3 \times 10^{-9} \text{ m}^2 \text{ s}^{-1}$, $D_{\text{Cl}^-} = 2.0 \times 10^{-9} \text{ m}^2 \text{ s}^{-1}$, and $D_{\text{OH}^-} = 5.3 \times 10^{-9}$.⁴⁶ The thermal diffusion factors are given by $\alpha_{\text{Na}^+}^\infty = 0.7$, $\alpha_{\text{Cl}^-}^\infty = 0.1$, $\alpha_{\text{OH}^-}^\infty = 3.4$.^{21,47,48} In all cases, we set $\varepsilon^* = 0$, dropping any thermal polarization effects, in order to facilitate the discussion of the results; the actual value $\varepsilon^* \approx -1.3$, see Appendix A.

7.2 The finite element method

We performed our finite-element calculations using the methods detailed in ref. 49 and previously utilized to study self-electrophoretic motion (without a temperature coupling) in ref. 38 and 50. We refer to those works for the details, briefly summarizing the key points here. (i) We exploit the rotational symmetry of our problem to work with an axisymmetric simulation domain on which the equations are specified in a manner that respects the three-dimensional nature of our problem. (ii) On this domain, we use a triangular mesh that grows out towards the edge of the domain in size. We improve the stability of our analysis using quadrilateral refinement in the region within several (typically 5) Debye lengths from the surface, see the appendix to ref. 38 for a visualization of such a domain. We ensured that our grids were sufficiently refined and our simulation domains sufficiently large to eliminate both discretization and finite-size effects, respectively. The discretization near the surface is typically less

than 0.01 of the particle radius, whilst the domains are at least than 30 particle radii in size. (iii) Polynomial basis functions were employed for the thermal, electrostatic, diffusion, and hydrodynamic subproblems, with orders 3 (Lagrange), 2, 3, and $3 + 2$, respectively. The latter refers to the order of the basis function for the velocity and pressure fields, respectively. (iv) To enhance stability and because the subproblems separate out in the low-Péclet regimes applicable here, we first solve for the temperature profile. This solution is used to subsequently compute the coupled electrostatic and diffusion problem, from which we obtain a force acting onto the fluid. Finally, the hydrodynamic problem with the appropriate boundary conditions is solved for the flow under the application of the obtained force. We measure the velocity of the fluid at the edge of our simulation domain – an average over the edge of the velocity – to work out the swim speed.

7.3 The temperature profile and thermocharge

Let us start by examining the temperature profile around a heated ($K = 1$) swimmer. Fig. 2 shows the temperature excess for both types of thermal boundary condition, where we chose the heat flux Q such that the maximum deviation from the reservoir temperature, $\Delta T \approx 5$ K, is comparable to the imposed excess temperature for the equi-temperature surface, $\Delta T = 5$ K. The two temperature fields differ only slightly.

Next, we turn our attention to the net charge at the surface of a hot ($K = 1$) swimmer with equipotential boundary condition, see Fig. 3. When the particle is not heated ($\Delta T = 0$ K), δX is fixed, and equal and opposite to the imposed value of ϕ_0 in our approximation. The agreement is good for $\phi_0 = 0.05$ (in the linear regime), but there is a substantial nonlinear effect for $\phi = 0.5$. The nonlinearity can be better captured analytically by using Poisson-Boltzmann theory.^{21,24} However, most of

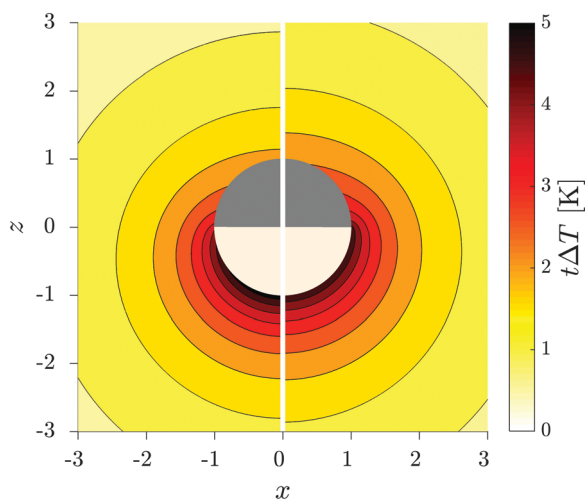


Fig. 2 Contour plot of the excess temperature $t\Delta T$ around a hot ($K = 1$) Janus swimmer in the xz -plane. In the left halfplane, we show t when the heat flux Q is fixed on the cap (white, $z \leq 0$), such that the maximum temperature on the capped hemisphere is ≈ 5 K. The right halfplane shows the temperature field with $\Delta T = 5$ K fixed on the heated cap.

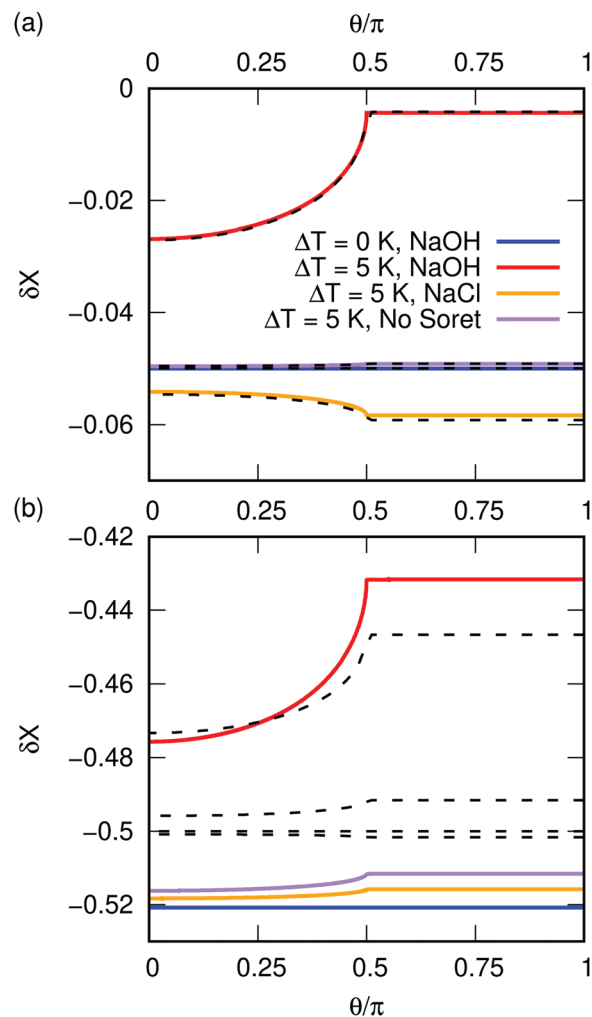


Fig. 3 The net charge $\delta X = \delta X^{\text{eq}} + \tau \delta X^{\text{neq}}$ along the particle contour parameterized by the polar angle θ . The curves are for a Janus swimmer with $\Delta T \approx 5$ K, $K = 1$, and an equipotential surface with $\phi_0 = 0.05$ (a) and $\phi_0 = 0.5$ (b); this corresponds to ≈ 2.6 mV and ≈ 13 mV, respectively. The black, dashed curves show the excellent agreement between our numerical result and analytic prediction.

the analytic manipulation performed in this paper cannot be (readily) accomplished in this more general case as the expressions become unwieldy.

Heating of the particle in a 1 mmol L^{-1} NaOH solution leads to an increase in the anion concentration at the hot surface. Recall that for $\varepsilon^* = 0$ the thermocharge at the surface is given by $\delta X^{\text{neq}} = (\phi_0 - \beta)t$ to first order, see eqn (30). Here, $\beta = -2.7$ and $\phi_0 = 0.05$, which gives $\delta X^{\text{neq}} = 2.75t$, and $\phi_0 = 0.5$, which gives $\delta X^{\text{neq}} = 3.2t$, respectively. Hence, we expect δX to increase at the heated cap – it is nearly constant over that hemisphere – and to be minimal at the pole of the particle, where the surface temperature is lowest.

The thermocharging effect is much smaller for a 1 mmol L^{-1} NaCl solution due to the smaller Soret coefficient of the Cl^- anion ($\beta = 0.6$); here we find $\delta X^{\text{neq}} = (\phi_0 - \beta)t = (0.05 - 0.6)t = -0.55t$ and $(0.5 - 0.6)t = -0.1t$, respectively. In the linear regime, our theory predicts the correct sign change of the

thermocharge with respect to the NaOH solution, but in the nonlinear regime there is no qualitative agreement. The reason for this is revealed by examining the situation where no Soret effect is included (purple curve). Here, we should obtain $\delta X^{\text{neq}} = \phi_0 t = 0.05t$ and $0.5t$, respectively. Clearly, the effect of nonlinearity is much stronger for the $\beta = 0$ thermocharging, as there is a sizable offset between the predicted δX and the computed one, see Fig. 3b.

7.4 The flow field around the hot swimmer

One of the most important properties of the swimmer is the flow field generated by the non-equilibrium effect, as this governs to first order the interaction of the swimmer with its environment. This aspect was previously explored by Bickel *et al.*³¹ for a hot swimmer that had a Seebeck-related slip velocity. Here, we include all terms leading to thermoelectric fluid motion in our equations and go beyond the Smoluchowski limit using FEM.

Fig. 4 shows representative flow fields for several swimmer and environmental configurations. We find that by lowering the salinity the puller type flow (butterfly shape) is suppressed, leaving a flow field that is more like that of a neutral squirmer. Changing the anion type and leaving the other parameters the same can be used to change the direction of motion and to change from a puller- to a pusher-type flow field, thereby strongly modifying the interaction of the hot swimmer with its environment.

The relatively high salinity used to generate the flow field in Fig. 4a, c and d most closely matches the conditions considered in ref. 31. Our flow field appears to qualitatively match their predictions. However, examining ref. 50–52 reveals that this shape is a generic feature of self-propulsion mechanisms which have a step-like change in boundary condition, be that step reactive or thermal in nature. That is, for a step-like change, there is a large gradient term that leads to an equally large velocity near the equator, which in turn strongly “compresses” the flow lines laterally, due to incompressibility of the medium.⁵¹ Thus, while there is a ‘match’ with the literature, the exact shape of the flow field is not particularly insightful. However, the puller *versus* pusher nature can be meaningfully distinguished.

Finally, we turn to the flow field shown in Fig. 4b. This flow does not have the butterfly shape, but is instead similar to that of a neutral squirmer. The step-like feature in the boundary condition is washed out, due to the size of the screening layer compared to that of the colloid at these low salt concentrations. Comparing our result to direct simulations of neutral self-thermophoresis reveals a similar flow field.⁵³ This correspondence is likely due to the weaker separation in scales in the simulations of ref. 53, *i.e.*, the solute species are small, but not very small compared to the size of the colloid.

7.5 Thermal conductivity and Soret coefficients

We start by providing the dimensionful expressions for the thermoelectrophoretic self-propulsion speed in the thin-screening-layer

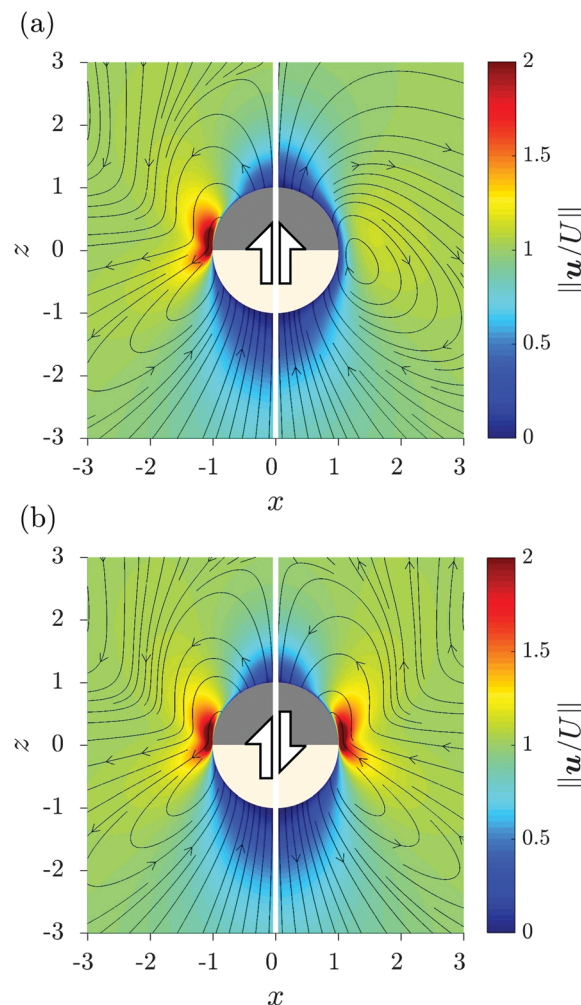


Fig. 4 Fluid velocity magnitude $\|\vec{u}\|$ divided by the absolute swim speed $|U|$ and streamlines for several hot ($K = 1$) swimmers in the laboratory frame of reference. In (a), the electrostatic potential is fixed at $\phi_0 = 0.5$ (≈ 13 mV) and we impose $\Delta T = 5$ K at the heated cap. The concentration of NaOH is 1 mmol L^{-1} in the left panel and $1 \times 10^{-3} \text{ mmol L}^{-1}$ in the right panel. In (b), the surface charge of the particle is fixed at $5 \times 10^{-3} e \text{ nm}^{-2}$ and $\Delta T = 5$ K. The electrolyte in the left panel is 1 mmol L^{-1} NaOH and, while in the right panel it is 1 mmol L^{-1} NaCl. Notice the opposite direction of the streamlines in the two panels as the swimmers translate in opposite directions. The large arrows in the center of the swimmer indicate the direction of motion.

limit here. These can be obtained by multiplying \bar{U} (eqn (48)) with $\Delta T/T^\infty$ and using Appendix B:

$$U = -\frac{k_B T^\infty n^\infty}{6\pi\eta^\infty a} (\lambda^\infty)^2 [8\beta\phi_i - \phi_i^2] \times \begin{cases} \frac{\Delta T}{T^\infty} & \text{isothermal cap} \\ \frac{3\pi a Q}{4k_f(2+K)T^\infty} & \text{constant heat flux cap} \end{cases} \quad (72)$$

Note that the dimensionful expression for the constant heat flux condition Q is not dependent on the particle radius a here. However, this is not the case in practice, since typically Q

depends on a . In general, $Q \propto I\sigma_{\text{abs}}/a^2$, where I is the illumination intensity and σ_{abs} is the absorption cross section. The dependence of σ_{abs} on a , however, is non-trivial. $\sigma_{\text{abs}} \propto a^3$ for small particles with $a \sim \mathcal{O}(0.01 \mu\text{m})$, while for big particles with $a \sim \mathcal{O}(10 \mu\text{m})$, $\sigma_{\text{abs}} \propto a^2$.⁵⁴ Therefore, Q varies from $Q \propto I/a$ to $Q \propto I$, while being more complex in between. We only consider a fixed value of a here and will ignore such dependencies in the following.

Fig. 5 shows the swim speed as a function of the bulk salt concentration for four representative swimmer/salt combinations and an equipotential boundary condition. The effect of the difference in thermal conductivity is quantitative, leading to an appreciable increase in absolute speed with reduced K . The direction of swimming is reversed between the two types of salt, as shown in Fig. 4 and previously reported by Ly *et al.*²⁴ In all cases we obtain significant swimming speeds, $\mathcal{O}(1 \mu\text{m s}^{-1})$, in physiological to high salt concentrations.

Note that we accurately capture the analytic Smoluchowski limit for our equipotential swimmer, even though we do not resolve the thermocharge correctly, see Fig. 3. In the analytic theory we find that for such a swimmer $U \propto n^\infty (\lambda^\infty)^2 \propto 1$ (in terms of n^∞). Our result implies that the swim speed is independent of the reservoir concentration to first order. This is borne out by our numerical data in Fig. 5, which is almost constant over a large range in n^∞ . Higher-order terms would capture the departures from the constant value of U close to the limit $\lambda^\infty \downarrow 0$. However, it is non-trivial to analyze these, as follows from Sections 5 and 6. We will analyze correspondence between analytic theory and numerical calculations in the Hückel limit in the next section.

The physical interpretation of the near-constant value of the speed is that smaller fluid velocities can be generated

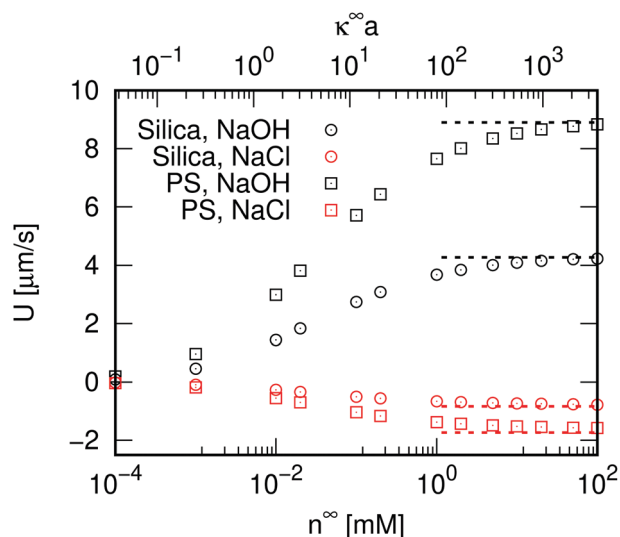


Fig. 5 Swimmer speed U as a function of the bulk salt concentration n^∞ for two electrolytes, NaOH (black) and NaCl (red), and two materials which comprise the hot swimmer, SiO_2 (circles) and PS (squares). As before, $\phi_0 = 0.5$ (≈ 13 mV) and we used a constant heat-flux boundary condition such that $\Delta T = 5$ K. The Debye length decreases towards the right and dashed lines indicate the analytic limit $\lambda^\infty \downarrow 0$.

in a thinner screening layer. However, this is exactly counterbalanced by the increased steepness of the electrostatic potential therein, which in itself leads to higher speeds. Whenever $\beta = 0$, the ion variation is in the bulk couples back to the surface, resulting in a dependency $U \propto \phi_0^2$, but with the same constancy in n^∞ .

7.6 Conducting and insulating hot swimmers

Fig. 6 shows the effect of the electrostatic boundary condition and the Soret effect on the motion of the hot swimmers as a function of the bulk salt concentration. Comparing the two panels of Fig. 6, the impact of the surface properties on the swim speed becomes evident.

As before, equipotential swimmers have nearly constant swim speed in the thin-screening-layer limit, see Fig. 6a.

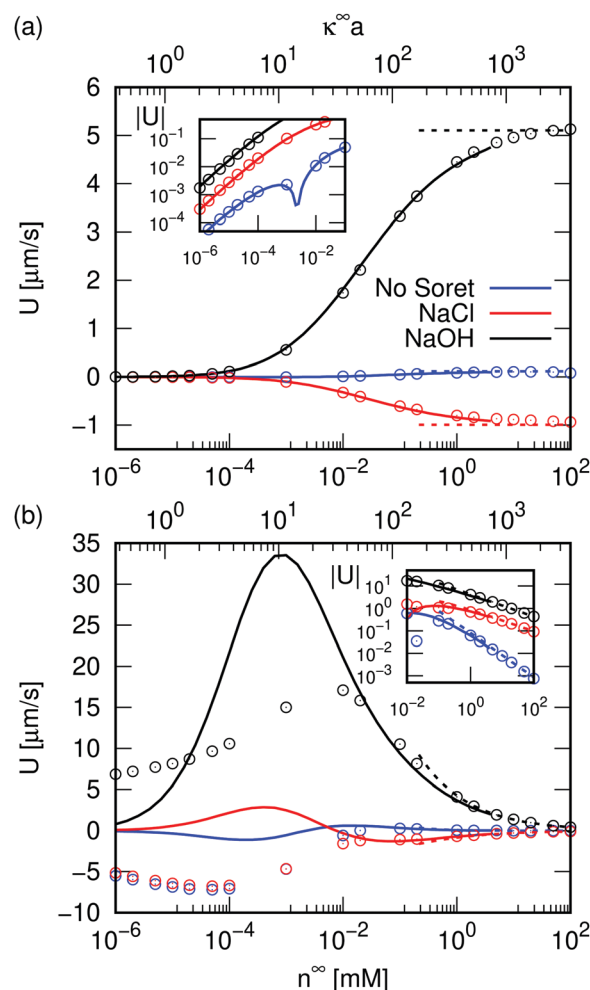


Fig. 6 Silica swimmer speed U as a function of salt concentration n^∞ for two electrolytes, NaCl (red) and NaOH (black), and when the Soret effect is neglected ($\beta = \gamma = 0$; blue). Symbols indicate the FEM result, solid curves show the analytic theory of Section 6, dashed lines the departure from the limiting value (eqn (48)). In (a) we use an equipotential electrostatic boundary condition with $\phi_0 = 0.5$ (≈ 13 mV), while in (b) we used a constant surface charge boundary condition $\sigma = 5 \times 10^{-3} e \text{ nm}^{-2}$. In both panels $\Delta T = 5$ K is fixed at the heated cap. The dashed lines indicate the prediction of eqn (48). The insets show the agreement between theory and numerical results in the Hückel (a) and Smoluchowski limit (b).

However, the speed of an insulating swimmer drops to zero in this limit. Note the excellent agreement between our analytic expressions and the FEM results here, see the inset to Fig. 6b. This is mathematically interpreted as follows. The surface potential ϕ_s corresponding to this boundary condition varies with the ion concentration, *i.e.*, $\phi_s \propto \lambda^\infty$. Thus, $U \propto n^\infty (\lambda^\infty)^3 \propto (n^\infty)^{-1/2}$ ($\beta \neq 0$) and $U \propto (n^\infty)^{-1}$ ($\beta = 0$) to first order, as can be appreciated from Fig. 6b. The physical intuition is that the surface potential must decrease with the Debye length in order to maintain the gradient-based boundary condition. Consequently, the coupling between the electric field and the temperature-induced ion currents reduces proportionally, leading to a vanishing speed.

Turning to the opposite limit of $n^\infty \downarrow 0$, *i.e.*, the Hückel limit, an equipotential swimmers' speed drops to zero, see Fig. 6a. This agrees with the result of eqn (61) which predicts a dependence $U \propto n_0$. In fact, the inset to Fig. 6a shows that the agreement is even quantitative. The physical interpretation of this scaling is as follows. Any n^∞ perturbation the unscreened potential, will predominantly generate an out-of-equilibrium ion profile, rather than directly screen the potential, which results in a linear dependence. Surprisingly, our analytic result holds for all intermediate ionic strengths that we considered. This indicates that our numerical results are trustworthy.

Fig. 6b shows that insulating swimmers have sizable speeds for low ionic strengths, which are only weakly dependent on the salt concentration over several decades (numerical result). The poor match between our analytic and numerical result for intermediate to low ionic strengths is expected, as the Debye-Hückel approximation breaks down in this regime for insulating surfaces. That is, nonlinearities must be accounted for to accurately capture the physics in this regime. However, we have verified that the numerical results, which account for such nonlinearities, are robust.

Physically, the surface-charge boundary condition imposes that a finite surface potential is maintained, which then couples to the few ions in the surrounding medium that maintain it. It may be that for even lower salt concentrations than considered here, the speed does decay to zero, though it seems unlikely considering the trend. We have chosen not to explore this limit for two reasons: (i) Much lower salt concentrations than studied in Fig. 6 are not attainable in aqueous experiments, due to water auto-dissociation and CO_2 dissolving in water and leading to a reduction in pH. (ii) Numerically it becomes increasingly difficult to solve the equation system without incurring finite-size or discretization artifacts for even lower ionic strength.

Observe that mobility reversals that are present both in our FEM calculations and our analytic theory for both conducting and insulating swimmers. This reversal is best observed for the former in the inset to Fig. 6a. Such reversals are reminiscent of external electrophoresis³⁰ and presumably have the same non-linear origin. This is why they only show up for $\beta = 0$ in the case of a conducting swimmer. For external thermoelectrophoresis, Burelbach and Stark observe a similar inversion as a function of the Debye length,²⁵ which could be attributed to the

same mechanism. However, we wish to emphasize that there are geometric differences between self- and external thermoelectrophoresis, hindering a direct comparison of the mobility inversion.

7.7 Mixed electrostatic boundary conditions

In experiment, metal-coated hot swimmers can possess more complex electrostatic boundary conditions than we have thus far considered. These hot Janus swimmers may be partially conducting and partially insulating or even have some intermediate form of boundary condition, due to sputter coating of the cap material, *e.g.*, see ref. 24. In this final results section, we analyze two systems, one where the capped side of the swimmer is a conductor and the uncapped side an insulator and the other with the opposite combination. Here, we focus on NaOH as the source of our Soret effect, as this gives the highest swim speeds.

Fig. 7 shows a comparison between homogeneous electrostatic surface boundary conditions for a hot swimmer (solid curves) and mixed ones (symbols). We find that the boundary condition on the uncapped half dominates the behavior in the Smoluchowski limit, as can be appreciated from the color inversion between the curves and symbols. This is expected for a fixed- ΔT boundary condition on the capped side in the Smoluchowski limit, as the only relevant temperature variation take place along the uncapped side in this case. For a constant heat-flux boundary condition on the cap, there would be a small contribution from the cap's electrostatic boundary condition.

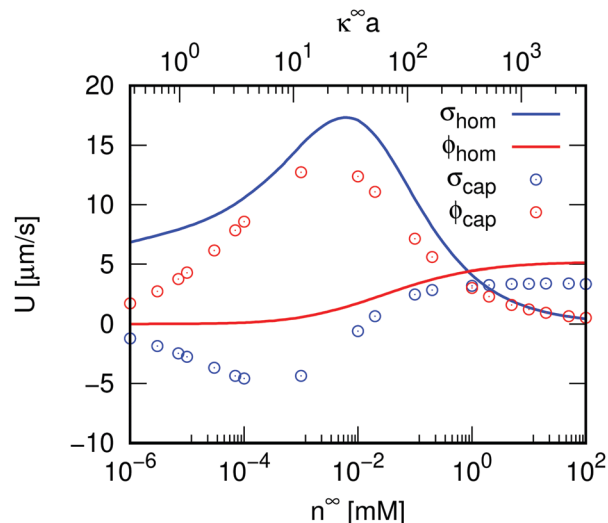


Fig. 7 Silica swimmer speed U as a function of salt concentration n^∞ for NaOH with homogeneous electrostatic boundary conditions (solid curves) and mixed boundary conditions (symbols). All results were obtained by FEM calculations for which $\Delta T = 5$ K is fixed at the heated cap. The solid curves belong to a homogeneous electrostatic boundary condition with $\phi_0 = 0.5$ (ϕ_{hom} ; red) and $\sigma = 5 \times 10^{-3} \text{ e nm}^{-2}$ (σ_{hom} ; blue). These curves correspond to a cubic interpolation of the data reported in Fig. 6. The red symbols (ϕ_{cap}) indicate a hot swimmer for which the capped side is an equipotential surface with $\phi_0 = 0.5$ and the uncapped side has a constant surface charge $\sigma = 5 \times 10^{-3} \text{ e nm}^{-2}$. The blue symbols (σ_{cap}) report the reverse mixed electrostatic boundary condition.

The deviation between the result for the homogeneous surface charge and equi-potential cap + insulating uncapped region can be attributed to the small region near the equator of the Janus particle, where the gradients are significant.

The results for the Hückel limit tend in the direction of the homogeneous equipotential speed (zero for $\lambda^\infty \uparrow \infty$) in both cases. This suggests that the sizable self-propulsion speed at low ionic strength that we reported in the last section can possibly only be achieved if the entire colloid behaves as an insulating surface. Such a homogeneous electrostatic boundary condition may be difficult to realize experimentally, though a carbon-coated particle may go in this direction. Lastly, note that for the case of an insulating cap and conducting uncapped region, a substantial mobility reversal at intermediate ionic strength is found.

8 Discussion and outlook

Summarizing, we have numerically determined the self-thermo(di)electrophoretic propulsion speed of a hot swimmer for various boundary conditions and environmental parameters. Specifically, we examined the largely unexplored regime of wide electrostatic screening layers (low ionic strength) using the finite-element method and verified our results in the appropriate limits using linear analytic theory, where possible.

We discussed in depth the limitations of the Debye–Hückel approximation for the case of an insulating swimmer in the electrostatic Hückel limit. In addition, the strengths and weaknesses of our various analytic approaches have been thoroughly charted. Despite the relatively strong reductions in our analytic theory, we were able to (semi-)quantitatively capture the speed dependence found by FEM in the Hückel limit for conducting swimmers over the full range of ionic strength that is relevant to aqueous systems. Fortuitously, our analytic expressions appear hold up to reasonably high values of the surface potential. However, more involved non-linear calculations are required to obtain better correspondence between analytic theory and numerical calculation for insulating swimmers in the Hückel limit.

Turning to the physics, we obtained $\mu\text{m s}^{-1}$ swimming speeds in physiological salt concentrations $n^\infty \gtrsim 1 \text{ mmol L}^{-1}$ for an equipotential boundary condition. These speeds are nearly independent of the salt concentration, in the thin screening-layer limit, due to a cancellation of ion-dependencies. For an insulating swimmer, however, propulsion speeds are low in this regime and they drop off with increasing bulk salinity. Counterintuitively, the speeds for an insulating swimmer appear to be nearly constant and are considerable in the limit of large Debye lengths, even without the thermoelectrophoretic effect taken into account. Presumably, this is a result of the need to have a small number of ions present to realize the boundary condition, even close to the Hückel limit. Analysis of systems with mixed electrostatic boundary conditions indicate that this result is not obtained therein, which suggest that it could be singular and experimentally difficult to realize. Between these two limits the direction of

self-propulsion can reverse, as clearly evidenced by our FEM calculations and supported by our analytic results.

To the best of our knowledge the low-salinity limit has not yet been systematically explored experimentally. Speculating on possible relations to reported experimental results, we note Simoncelli *et al.*¹⁶ observed a decrease of the height above the surface for their thermophoretic swimmers with increased salt concentration. However, these authors study a system wherein the particle's self-propulsion is directed towards/away from a nearby wall. This complicates direct interpretation of the results in terms of a swim speed, as near-surface thermo-electroosmotic couplings may come into play. Nonetheless, the observed decrease in height by switching from NaCl to NaOH could be related to a reversal in swim direction when using this salt,¹⁶ potentially in agreement with our results, as well as those of ref. 24. In addition, the decrease in height with increased salt concentration may be related to the conductivity of the cap, as we have observed for the mixed boundary conditions.

The main takeaway message of our work is that there may be interesting nonlinearities in the motility of self-thermo(di)-electrophoretic colloids that can be induced by varying the salt concentration in an experimentally accessible range. The FEM method is particularly well suited to study this range, though analytic progress may be made. Full analysis of the impact of non-uniformities in terms of the surface boundary conditions on the swim speed over the full range of experimentally accessible ionic strengths is left to future study.

Author contribution

Numerical calculations S. S. and analytic theory J. d. G.

Conflicts of interest

There are no conflicts to declare.

Appendix A: justification of linearization

In this appendix, we justify the reductions we made in the main text. We refer to the work by Dietzel and Hardt²³ and references therein for a full discussion of the first-order Taylor expansion coefficients to the physical quantities. Here, we reproduce the values listed in ref. 23 in terms of our notation. For the medium they found $\eta^* \approx -5$, $k^* \approx 0.7$, and $\varepsilon^* \approx -1.3$. For the “typical” ions Na^+ , K^+ , and Cl^- they obtained $D_\pm^* \approx 6$.²³ For the variation in the thermal diffusion factors of the ions only limited data is available in the literature. We refer to the work of Caldwell,⁵⁵ from which we obtain $D_\pm^* \approx 1$ for NaCl and a temperature dependence for the thermal diffusion factor given by $\alpha_\pm^* \approx 2$. There is clearly some variation in the literature values, but importantly all these numbers are order unity and we are therefore justified in ignoring these temperature dependencies. They come into the differential equations for the potential and concentration at $\mathcal{O}(\tau^2)$, with $\tau^2 \approx 3 \times 10^{-4}$ for $\Delta T \leq 5 \text{ K}$, leading

to minute variations. For the speed they come into the expression at $\mathcal{O}(\tau)$, which leads to a change of at most 10%. The only exception to this rule is ε^* , which enters the theory at linear order and contributes as a constant to the speed, see eqn (72). Finally, the Péclet number for the ions in our system is given by $Pe = Ua/D$, with $U \leq 10 \mu\text{m s}^{-1}$ the typical velocity, $a = 1 \mu\text{m}$ the radius of the colloid, and $D \geq 1.0 \times 10^{-9} \text{m}^2 \text{s}^{-1}$ the smallest ion diffusion coefficient for convenience. Using the numbers provided in Section 7, we find that $Pe \leq 10^{-2}$, therefore we can safely ignore advective terms in eqn (20). Similarly, we can ignore thermal advection terms, since thermal diffusion is orders of magnitude larger than regular ion diffusion.

Appendix B: temperature profiles

We follow ref. 31 to obtain the temperature profiles in our system and reproduce their results here in our notation for completeness. We examine two boundary conditions for the coated hemisphere. For the a cap maintained at constant temperature, we assume for the thermal conductivities $k_f = k_s$, and obtain for the reduced temperature field $t(\vec{r})$ outside of the swimmer

$$t(\vec{r}) = \frac{1}{2} \left(\frac{a}{r} \right) + \sum_{i=0}^{\infty} \bar{t}_i \left(\frac{a}{r} \right)^{i+1} P_i(\cos \theta), \quad (73)$$

$$\bar{t}_{i=2k} = \frac{1}{\pi} \frac{(-1)^k}{2k+1}, \quad (74)$$

$$\bar{t}_{i=2k+1} = -\frac{1}{\pi} \frac{(-1)^k}{2k+1}, \quad (75)$$

where, P_i is the i -th Legendre polynomial.

For a constant heat flux Q into the cap, the dimensionful temperature field $T(\vec{r})$ reads

$$T(\vec{r}) = T^\infty + \frac{aQ}{2k_f} \left[\left(\frac{a}{r} \right) + \sum_{i=0}^{\infty} \hat{t}_i \left(\frac{a}{r} \right)^{i+1} P_i(\cos \theta) \right], \quad (76)$$

$$\hat{t}_{i=2k} = 0, \quad (77)$$

$$\hat{t}_{i=2k+1} = -\frac{4k+3}{(2k+2) + (2k+1)K} \frac{(-1)^k (2k)!}{2^{2k+1} k! (k+1)!}, \quad (78)$$

where $K = k_s/k_f$ is the conductivity contrast. In this case, the maximum temperature difference appearing in our τ expansion can be written as

$$\Delta T = \frac{aQ}{2k_f} \left[1 - \sum_{i=0}^{\infty} \hat{t}_i \right], \quad (79)$$

leading to a reduced temperature field $t(\vec{r})$ that may be written in a more convenient form for our purposes,

$$t(\vec{r}) = \left(\frac{a}{r} \right) \left[1 - \sum_{j=0}^{\infty} \hat{t}_j \right]^{-1} + \sum_{i=0}^{\infty} \bar{t}_i \left(\frac{a}{r} \right)^{i+1} P_i(\cos \theta), \quad (80)$$

$$\bar{t}_i = \hat{t}_i \left[1 - \sum_{j=0}^{\infty} \hat{t}_j \right]^{-1}. \quad (81)$$

Appendix C: the equilibrium solutions

The linearized equations for the equilibrium in terms of our reduced quantities are as follows. The heat equation reduces to a constant temperature T^∞ throughout the system. The Stokes equations reduce to zero fluid velocity, with the following pressure condition

$$\vec{\nabla} p^{\text{eq}}(\vec{r}) = -k_B T^\infty n^\infty (x_+^{\text{eq}}(\vec{r}) - x_-^{\text{eq}}(\vec{r})) \vec{\nabla} \phi^{\text{eq}}(\vec{r}). \quad (82)$$

That is, the hydrostatic pressure exactly cancels the ionic pressure terms induced by electrostatic screening of any charge or potential on the colloid. The linearized equilibrium Poisson equation reads

$$\nabla^2 \phi^{\text{eq}}(\vec{r}) = -\frac{1}{2} (\kappa^\infty)^2 (x_+^{\text{eq}}(\vec{r}) - x_-^{\text{eq}}(\vec{r})). \quad (83)$$

Lastly, the ionic fluxes become

$$\vec{j}_\pm^{\text{eq}}(\vec{r}) = -D_\pm^\infty n^\infty \left[\vec{\nabla} x_\pm^{\text{eq}}(\vec{r}) \pm \vec{\nabla} \phi^{\text{eq}}(\vec{r}) \right], \quad (84)$$

with the closure $\vec{j}_\pm^{\text{eq}}(\vec{r}) = \vec{0}$. The latter follows from the fact that in equilibrium the fluxes vanish. Using the closure, we find that $x_\pm^{\text{eq}}(\vec{r}) = \mp \phi^{\text{eq}}(\vec{r})$ and $\nabla^2 \phi^{\text{eq}}(\vec{r}) = (\kappa^\infty)^2 \phi^{\text{eq}}(\vec{r})$. The hydrostatic pressure condition reduces to $\vec{\nabla} p^{\text{eq}}(\vec{r}) = 2k_B T^\infty n^\infty \phi^{\text{eq}}(\vec{r}) \vec{\nabla} \phi^{\text{eq}}(\vec{r})$.

Appendix D: the expansion of Teubner's integration

We rewrite the expression for the speed given by Teubner,³² see eqn (49), in terms of the body force inside and outside the screening layer – using that the latter is vanishing and that the system is axisymmetric – to arrive at

$$\begin{aligned} \bar{U} &= \frac{1}{3\eta^\infty a} \int_a^\infty r^2 \int_0^\pi \sin \theta \underline{K}(\vec{r}) \cdot \vec{f}^{\text{neq}}(\vec{r}) d\theta dr \\ &= \frac{1}{3\eta^\infty a} \int_a^{a^+} r^2 \int_0^\pi \sin \theta \underline{K}(\vec{r}) \cdot \vec{f}_{\text{in}}^{\text{neq}}(\vec{r}) d\theta dr, \end{aligned} \quad (85)$$

where a^+ marks the edge of the screening layer. We have that $\underline{K}(\vec{r}_s) = \vec{0}$ and we must therefore perform a perturbative analysis in terms of $\lambda^\infty/a \ll 1$ to obtain the relevant weighting factors over the length of the screening layer. We introduce $\vec{r} = \vec{r}_s + \lambda^\infty \vec{q}\hat{q}$, such that

$$\begin{aligned} \bar{U} &= \frac{\lambda^\infty}{3\eta^\infty a} \int_0^\pi \int_0^\pi (a + \lambda^\infty q)^2 \sin \theta \underline{K}(\vec{r}_s + \lambda^\infty q\hat{q}) \\ &\quad \times \vec{f}_{\text{in}}^{\text{neq}}(\vec{r}_s + \lambda^\infty q\hat{q}) d\theta dq, \end{aligned} \quad (86)$$

where the λ^∞ term comes from the Jacobian of the coordinate transformation and we have taken the limit to infinity for the q integration, as $a^+ = \lim_{q \uparrow \infty} a + \lambda^\infty q$. The expressions for the terms that do not pertain to the force reduce to

$$\begin{aligned} &\frac{\lambda^\infty}{3\eta^\infty a} (a + \lambda^\infty q)^2 \sin \theta \underline{K}(\vec{r}_s + \lambda^\infty q\hat{q}) \\ &= -\frac{(\lambda^\infty)^3 q^2}{2\eta^\infty a} \cos \theta \sin \theta \hat{q} + \frac{(\lambda^\infty)^2 q}{2\eta} \sin^2 \theta \hat{\theta}, \end{aligned} \quad (87)$$

to leading order in λ^∞ . We verified that the next order terms do not contribute to the speed at leading order. For the force, we obtain

$$\vec{f}_{\text{in}}^{\text{neq}}(\vec{r}_s + \lambda^\infty q \hat{q}) = A(q) \hat{q} t(a, \theta) + B(q) a^{-1} \hat{\theta} \partial_\theta t(a, \theta), \quad (88)$$

where the term $t(a, \theta) \equiv t(\vec{r}_s)$ is the temperature at the surface. Here, $A(q)$ accounts for all the prefactors in eqn (38) and (39); $B(q)$ accounts for all the relevant prefactors in eqn (40) and (41); and $a^{-1} \hat{\theta} \partial_\theta t(a, \theta) \equiv \vec{\nabla}_\parallel t(\vec{r}_s)$. Note that here we have used our assumption that $\phi(\vec{r}_s)$ is homogeneous over the surface to avoid q dependence in the factors A and B .

Now taking everything together, we may rewrite the expression for the speed contribution due to the region inside of the thin screening layer as

$$\begin{aligned} \bar{U} \approx & \frac{(\lambda^\infty)^2}{2\eta^\infty a} \int_0^\infty \int_0^\pi [\lambda^\infty q^2 \cos \theta \sin \theta A(q) t(a, \theta) \\ & - q \sin^2 \theta B(q) \partial_\theta t(a, \theta)] d\theta dq. \end{aligned} \quad (89)$$

Spitting the integrand into the $A(q)$ (\perp) and $B(q)$ (\parallel) terms, we evaluate these contributions separately. Starting with the perpendicular component, we find

$$\begin{aligned} \bar{U}_\perp &= \frac{(\lambda^\infty)^3}{2\eta^\infty a} \int_0^\infty \int_0^\pi q^2 \cos \theta \sin \theta A(q) t(a, \theta) d\theta dq \\ &= \frac{(\lambda^\infty)^3}{2\eta^\infty a} \int_0^\infty q^2 A(q) dq \int_0^\pi t(a, \theta) \cos \theta \sin \theta d\theta \\ &= \frac{(\lambda^\infty)^3}{3\eta^\infty a} \bar{t}_1 \int_0^\infty q^2 A(q) dq, \end{aligned} \quad (90)$$

where only the first-order Legendre Polynomial contributes. Note that if we had not assumed homogeneous electrostatic surface properties, the splitting of the integration could not have been done in the same way and all Legendre–Fourier modes would have contributed. Evaluating the integral over q gives us for a conducting surface

$$\bar{U}_\perp = -\frac{k_B T^\infty n^\infty}{6\eta^\infty a} (\lambda^\infty)^2 [2\beta\phi_0 + \varepsilon^* \phi_0^2] \bar{t}_1. \quad (91)$$

The result for an insulating surface is

$$\bar{U}_\perp = -\frac{k_B T^\infty n^\infty}{6\eta^\infty a} (\lambda^\infty)^2 [1 + 2\varepsilon^*] \phi_s^2 \bar{t}_1. \quad (92)$$

Similarly, we obtain for the parallel component

$$\begin{aligned} \bar{U}_\parallel &= \frac{(\lambda^\infty)^2}{2\eta^\infty a} \int_0^\infty \int_0^\pi q \sin^2 \theta B(q) \partial_\theta t(a, \theta) d\theta dq \\ &= \frac{(\lambda^\infty)^2}{2\eta^\infty a} \int_0^\infty q B(q) dq \int_0^\pi \sin^2 \theta \partial_\theta t(a, \theta) d\theta \\ &= -\frac{2(\lambda^\infty)^2}{3\eta^\infty a} \bar{t}_1 \int_0^\infty q B(q) dq. \end{aligned} \quad (93)$$

Evaluating the integral over q leads to the desired expression for a conducting surface

$$\bar{U}_\parallel = -\frac{k_B T^\infty n^\infty}{6\eta^\infty a} (\lambda^\infty)^2 [6\beta\phi_0 - \phi_0^2] \bar{t}_1, \quad (94)$$

and for an insulating surface

$$\bar{U}_\parallel = -\frac{k_B T^\infty n^\infty}{6\eta^\infty a} (\lambda^\infty)^2 [8\beta\phi_s - (2 + \varepsilon^*) \phi_s^2] \bar{t}_1. \quad (95)$$

Appendix E: solving the general differential form

We write a general Legendre–Fourier series for the reduced temperature, mimicking the result obtained in Appendix C. That is,

$$t(\vec{r}) = \sum_{j=0}^{\infty} \check{t}_j y^{-(j+1)} P_j(\cos \theta), \quad (96)$$

with P_i the i -th Legendre polynomial and the \check{t}_j prefactors of the temperature expansion that can be related to the \bar{t}_j provided in Appendix B. Then, the general differential form associated with our splitting approach may be recast as

$$\nabla^2 G(\vec{r}) = g \vec{\nabla} t(\vec{r}) \cdot \vec{\nabla} \phi^{\text{eq}}(\vec{r}), \quad (97)$$

with G a function and g some prefactor. The gradient of the equilibrium potential only has a radial component, under our constraining assumptions, therefore

$$\nabla^2 G(\vec{r}) = g \check{\phi}_s \sum_{j=0}^{\infty} \check{t}_j (j+1) y^{-(j+4)} P_j(\cos \theta). \quad (98)$$

A solution to this problem should also decompose into Legendre–Fourier modes, hence we make the ansatz

$$G(\vec{r}) = \sum_{j=0}^{\infty} h_j(y) P_j(\cos \theta), \quad (99)$$

with h_j functions to be determined. From eqn (98) and (99) it then follows that the h_j satisfy

$$h_j''(y) + \frac{2}{y} h_j'(y) - \frac{j(j+1)}{y^2} h_j(y) = g \check{\phi}_s \check{t}_j \frac{(j+1)}{y^{(j+4)}}, \quad (100)$$

with the prime denoting the derivative with respect to y . These differential equations have solutions

$$h_j(y) = \left(\frac{1}{2} g \check{\phi}_s \check{t}_j + C_j y \right) y^{-(j+2)}, \quad (101)$$

where the C_j are constants of integration to be determined. We have removed the nonconvergent part in the limit of $y \uparrow \infty$, since we are interested in the limit $\xi^{-1} \uparrow \infty$ and the solutions should be bounded for all ξ .

Acknowledgements

We thank Marie Skłodowska-Curie Intra European Fellowship (G. A. No. 654916, JdG, and 656327, SS) within Horizon 2020

for funding. JdG further acknowledges funding through association with the EU-FET project NANOPHLOW (766972) within Horizon 2020. We are grateful to Aidan Brown, Mathijs Janssen, Willem Boon, and Ben Werkhoven for fruitful discussions.

Notes and references

- W. Paxton, K. Kistler, C. Olmeda, A. Sen, S. St. Angelo, Y. Cao, T. Mallouk, P. Lammert and V. Crespi, *J. Am. Chem. Soc.*, 2004, **126**, 13424.
- J. R. Howse, R. A. Jones, A. J. Ryan, T. Gough, R. Vafabakhsh and R. Golestanian, *Phys. Rev. Lett.*, 2007, **99**, 048102.
- M. Marchetti, J.-F. Joanny, S. Ramaswamy, T. Liverpool, J. Prost, M. Rao and R. Simha, *Rev. Mod. Phys.*, 2013, **85**, 1143.
- I. Theurkauff, C. Cottin-Bizonne, J. Palacci, C. Ybert and L. Bocquet, *Phys. Rev. Lett.*, 2012, **108**, 268303.
- J. Palacci, S. Sacanna, A. Steinberg, D. Pine and P. Chaikin, *Science*, 2013, **339**, 936–940.
- I. Buttinoni, J. Bialké, F. Kümmel, H. Löwen, C. Bechinger and T. Speck, *Phys. Rev. Lett.*, 2013, **110**, 238301.
- W. Duan, R. Liu and A. Sen, *J. Am. Chem. Soc.*, 2013, **135**, 1280.
- D. Singh, U. Choudhury, P. Fischer and A. Mark, *Adv. Mater.*, 2017, **29**, 1701328.
- W. Gao, A. Pei, R. Dong and J. Wang, *J. Am. Chem. Soc.*, 2014, **136**, 2276.
- C. Zhou, H. Zhang, J. Tang and W. Wang, *Langmuir*, 2018, **34**, 3289.
- K. Dey, X. Zhao, B. Tansi, W. Méndez-Ortiz, U. Córdoba-Figueroa, R. Golestanian and A. Sen, *Nano Lett.*, 2015, **15**, 8311.
- X. Ma, X. Wang, K. Hahn and S. Sánchez, *ACS Nano*, 2016, **10**, 3597.
- H.-R. Jiang, M. Yoshinaga and N. Sano, *Phys. Rev. Lett.*, 2010, **105**, 268302.
- I. Buttinoni, G. Volpe, F. Kümmel, G. Volpe and C. Bechinger, *J. Phys.: Condens. Matter*, 2012, **24**, 284129.
- L. Baraban, R. Streubel, D. Makarov, L. Han, D. Karnausenko, O. Schmidt and G. Cuniberti, *ACS Nano*, 2013, **7**, 1360.
- S. Simoncelli, J. Summer, S. Nedeve, P. Kühler and J. Feldmann, *Small*, 2016, **12**, 2854.
- R. Piazza and A. Parola, *J. Phys.: Condens. Matter*, 2008, **20**, 153102.
- J. Burelbach, D. Frenkel, I. Pagonabarraga and E. Eiser, *Eur. Phys. J. E: Soft Matter Biol. Phys.*, 2018, **41**, 7.
- J. Dhont, S. Wiegand, S. Duhr and D. Braun, *Langmuir*, 2007, **23**, 1674.
- J. Dhont and W. Briels, *Eur. Phys. J. E: Soft Matter Biol. Phys.*, 2008, **25**, 61.
- A. Majee and A. Würger, *Phys. Rev. Lett.*, 2012, **108**, 118301.
- M. Dietzel and S. Hardt, *Phys. Rev. Lett.*, 2016, **116**, 225901.
- M. Dietzel and S. Hardt, *J. Fluid Mech.*, 2017, **813**, 1060.
- A. Ly, A. Majee and A. Würger, *New J. Phys.*, 2018, **20**, 025001.
- J. Burelbach and H. Stark, *Eur. Phys. J. E: Soft Matter Biol. Phys.*, 2019, **42**, 1.
- S. Samin and R. van Roij, *Phys. Rev. Lett.*, 2015, **115**, 188305.
- B. Huang, M. Roger, M. Bonetti, T. Salez, C. Wiertel-Gasquet, E. Dubois, R. Cabreira Gomes, G. Demouchy, G. Mériquet, V. Peyre, M. Kouyaté, C. Filomeno, J. Depeyrot, F. Tourinho, R. Perzynski and S. Nakamae, *J. Chem. Phys.*, 2015, **143**, 054902.
- C. Filomeno, M. Kouyaté, V. Peyre, G. Demouchy, A. Campos, R. Perzynski, F. Tourinho and E. Dubois, *J. Phys. Chem. C*, 2017, **121**, 5539.
- R. Cabreira, A. da Silva Ferreira, M. Kouyaté, G. Demouchy, G. Mériquet, R. Aquino, E. Dubois, S. Nakamae, M. Roger, J. Depeyrot and R. Perzynski, *Phys. Chem. Chem. Phys.*, 2018, **20**, 16402.
- R. O'Brien and L. White, *J. Chem. Soc., Faraday Trans. 2*, 1978, 1607.
- T. Bickel, A. Majee and A. Würger, *Phys. Rev. E: Stat., Nonlinear, Soft Matter Phys.*, 2013, **88**, 012301.
- M. Teubner, *J. Chem. Phys.*, 1982, **76**, 5564.
- L. Landau, E. Lifshits and L. Pitaevskii, *Electrodynamics of continuous media*, Pergamon Press, Oxford, 1984, vol. 8.
- K. Morozov, *J. Exp. Theor. Phys.*, 1999, **88**, 944.
- S. Rasuli and R. Golestanian, *Phys. Rev. Lett.*, 2008, **101**, 108301.
- A. Würger, *Phys. Rev. Lett.*, 2008, **101**, 108302.
- J. Gomez-Solano, S. Samin, C. Lozano, P. Ruedas-Batuecas, R. van Roij and C. Bechinger, *Sci. Rep.*, 2017, **7**, 14891.
- A. Brown, W. Poon, J. Holm and C. de Graaf, *Soft Matter*, 2017, **13**, 1200.
- T. Ghonge, J. Chakraborty, R. Dey and S. Chakraborty, *Phys. Rev. E: Stat., Nonlinear, Soft Matter Phys.*, 2013, **88**, 053020.
- R. Stout and A. Khair, *Phys. Rev. E*, 2017, **96**, 022604.
- M. Janssen and M. Bier, *Phys. Rev. E*, 2019, **99**, 042136.
- B. Derjaguin and G. Sidorenkov, *Proc. USSR Acad. Sci.*, 1941, **32**, 622.
- J. Anderson, *Annu. Rev. Fluid Mech.*, 1989, **21**, 61.
- J. Brady, *J. Fluid Mech.*, 2011, **667**, 216.
- W. Haynes, D. Lide and T. Bruno, *Handbook of chemistry and physics: a ready-reference book of chemical and physical data*, CRC Press, Boca Raton, 2009, vol. 90.
- E. Samson, J. Marchand and K. Snyder, *Mater. Struct.*, 2003, **36**, 156.
- E. Eastman, *J. Am. Chem. Soc.*, 1928, **50**, 283.
- J. Agar, C. Mou and J. Lin, *J. Phys. Chem.*, 1989, **93**, 2079.
- G. Rempfer, G. Davies, C. Holm and J. de Graaf, *J. Chem. Phys.*, 2016, **145**, 044901.
- P. Kreissl, C. Holm and J. de Graaf, *J. Chem. Phys.*, 2016, **144**, 204902.
- J. de Graaf, G. Rempfer and C. Holm, *IEEE Trans. Nano-Biosci.*, 2015, **14**, 272.
- S. Reigh, M.-J. Huang, J. Schofield and R. Kapral, *Philos. Trans. R. Soc., A*, 2016, **374**, 20160140.
- M. Yang, A. Wysocki and M. Ripoll, *Soft Matter*, 2014, **10**, 6208.
- A. Bregulla and F. Cichos, *Faraday Discuss.*, 2015, **184**, 381.
- D. Caldwell, *Deep Sea Research and Oceanographic Abstracts*, 1973, p. 1029.